

Electromagnetic fields from the extended Kharzeev-McLerran-Warringa model in relativistic heavy-ion collisions

Yi Chen,^{1,2} Xin-Li Sheng,³ and Guo-Liang Ma^{4,1,*}

¹*Shanghai Institute of Applied Physics, Chinese Academy of Sciences, Shanghai 201800, China*

²*University of Chinese Academy of Sciences, Beijing 100049, China*

³*Key Laboratory of Quark and Lepton Physics (MOE) and Institute of Particle Physics, Central China Normal University, Wuhan 430079, China*

⁴*Key Laboratory of Nuclear Physics and Ion-beam Application (MOE), Institute of Modern Physics, Fudan University, Shanghai 200433, China*

Based on the Kharzeev-McLerran-Warringa (KMW) model that estimates the strong electromagnetic (EM) fields generated in relativistic heavy-ion collisions, we generalize the formulas of EM fields in the vacuum by incorporating the longitudinal position dependence, the generalized charge distributions and retardation correction. We further generalize the formulas of EM fields in the pure quark-gluon plasma (QGP) medium by incorporating a constant Ohm electric conductivity and also in the realistic early-stage QGP evolution by using a time-dependent electric conductivity. Using the extended KMW model, we observe a slower time evolution and a more reasonable impact parameter b dependence of the magnetic field strength than those from the original KMW model in the vacuum. The inclusion of medium effects by using the lattice results on conductivity helps further prolong the time evolution of magnetic field, such that the magnetic field strength during the QGP evolution at thermal freeze-out time can well satisfy and roughly approach the required magnetic field strength for the explanation of the observed difference in global polarizations of Λ and $\bar{\Lambda}$ hyperons in Au+Au collisions at top RHIC energy. These generalized formulations in the extended KMW model will be potentially useful for many EM fields relevant studies in heavy-ion collisions, especially at lower colliding energies and for various species of colliding nuclei.

I. INTRODUCTION

The study of strongly interacting matter and its properties in the presence of strong electromagnetic (EM) fields has been a hot topic for more than a decade [1–35]. The ultra-relativistic heavy-ion collisions provide a unique way for creating and exploring the strongly interacting matter at extremely high temperature and high energy density, where the matter is expected to be deconfined and reach a new state of matter, which is so-called the “quark-gluon plasma” (QGP) [36–39]. Properties of strongly interacting matter are governed by quantum chromodynamics (QCD), which have been widely and experimentally studied both on the Relativistic Heavy Ion Collider (RHIC) at Brookhaven National Laboratory (BNL) and on the Large Hadron Collider (LHC) at CERN. In heavy-ion collisions, e.g., at top RHIC energy at $\sqrt{s} = 200$ GeV or LHC energy at $\sqrt{s} = 5.02$ TeV, the two oppositely fast moving (almost at the speed of light) colliding nuclei in non-central nucleus-nucleus (A-A) collisions can generate hitherto the strongest EM fields [1–35], which are usually estimated to be at the order of magnitude of $eB \sim eE \sim m_\pi^2 \sim 10^{18}$ G at top RHIC energy, or $eB \sim eE \sim 10 m_\pi^2 \sim 10^{19}$ G at LHC energies, where m_π is the pion mass. Here we note that the event-by-event fluctuations of generated EM fields have been widely studied in Refs. [9–11, 15, 21–23, 29–34] in recent years, which can give rise to non-vanishing components of EM fields such as $|B_x|$ and $|E_x|$ due to the fluctuations of proton positions in the two colliding nuclei.

In the QCD vacuum, topologically non-trivial gluon field configuration with non-zero winding number Q_w [40–42] of deconfined QGP in the presence of such a strong magnetic field \mathbf{B} will induce a non-conserved axial current $j_\mu^5 = \sum_f q_f \langle \bar{\psi}_f \gamma_\mu \gamma^5 \psi_f \rangle_A$ as well as a vector current $j_\mu = \sum_f q_f \langle \bar{\psi}_f \gamma_\mu \psi_f \rangle_V$ along the direction of magnetic field, which are respectively called the “charge separation effect” (CSE) and the “chiral magnetic effect” (CME) [2, 6, 43–51]. Since the axial current j_μ^5 requires a charge imbalanced \mathcal{C} -odd environment while the vector current j_μ requires a chirality imbalanced \mathcal{P} -odd environment, an asymmetry between the amount of positive and negative charges along the direction of magnetic field \mathbf{B} in heavy-ion collisions is expected. Experimental observations of CME can be regarded as direct evidences of topologically non-trivial gluon field configurations, and furthermore can be interpreted as indications of event-by-event local \mathcal{P} and \mathcal{CP} violation of QCD at quantum level [2, 43].

*Electronic address: glma@fudan.edu.cn

Besides the CME and CSE, it is well known that strong magnetic fields can also influence many QCD processes [49], e.g. the induction of chiral symmetry breaking [52], the influences on chiral condensation [53], and the modification of in-medium particle's mass [54–60]. As an important consequence, the QCD phase diagram may be dynamically modified by such a strong magnetic field [61–65], e.g. color-superconducting phases at very high baryon densities will be strongly affected by the strong magnetic field [61]. When anomaly processes are coupled with strong magnetic fields, many interesting effects [49], e.g. the formation of π^0 -domain walls [66], will also be induced and generated.

Due to the fact that the generated magnetic field \mathbf{B} in heavy-ion collisions can not be directly measured event-by-event, it is of enormous challenge to measure the magnetic field \mathbf{B} induced chiral anomalous effects in current experiments. In heavy-ion collisions, the magnetic field \mathbf{B} is generated along the direction preferentially perpendicular to the reaction plane, hence experimental measurements are usually conducted using the two-particle correlators $\gamma_{\alpha\beta} = \langle\langle \cos(\phi_\alpha + \phi_\beta - 2\Psi_{\text{RP}}) \rangle\rangle$ firstly proposed by Voloshin [67], where α and β denote the electric charge sign of particles α and β , ϕ_α and ϕ_β are their azimuthal angles respectively, and Ψ_{RP} is the azimuthal angle of the constructed reaction plane for a given event, and $\langle\langle \cdots \rangle\rangle$ denotes the average over all particle pairs and then over all events. Therefore, the same-sign (SS) and opposite-sign (OS) correlators can be respectively written as $\gamma_{\text{ss}} \equiv (\gamma_{++} + \gamma_{--})/2$ and $\gamma_{\text{os}} \equiv (\gamma_{+-} + \gamma_{-+})/2$. Based on [5, 67], the magnetic field driven CME is expected to contribute to a negative γ_{ss} but a positive γ_{os} . The STAR Collaboration [68–73] and ALICE Collaboration [74] have independently measured the γ_{ss} and γ_{os} correlators, which indeed show the expected features of the CME. However, there exit some ambiguities [75–83] in the interpretation of the experimental data due to the large background contaminations, potentially arising from the elliptic-flow (v_2) driven background contributions, such as the transverse momentum conservation (TMC) [78, 82, 83], local charge conservation (LCC) [79–81]. Hence, a dedicated run of the $^{96}\text{Zr} + ^{96}\text{Zr}$ and $^{96}\text{Ru} + ^{96}\text{Ru}$ isobar colliding systems at RHIC has been proposed [5], which is expected to yield unambiguous evidence for the CME signal by varying the signal but with the v_2 -driven backgrounds roughly fixed [5, 84–89].

In this paper, we will review some generic features of an analytical model for the estimation of EM fields generated in relativistic heavy-ion collisions from the original work initiated by Kharzeev, McLerran and Warringa [2], which we refer to as the original KMW model. On the ground of it, we formulate our generalizations of the estimated EM fields. We first start from the generalization of charge distributions used in heavy-ion collisions, based on which we point out that the formulas of EM fields in the original KMW model can be properly extended by incorporating the longitudinal position dependence through the generalized relativistic three-dimensional charge distribution models, e.g., three-parameter Fermi (3pF) model, for both spherically symmetric colliding nuclei and axially deformed ones. Also, we make the retardation correction (RC) to the estimated EM fields contributed by participants, such that our formulation of the estimated EM fields can be potentially applied to lower energy region, such as the current beam-energy-scan (BES) program at RHIC, the under planning FAIR, NICA and J-PARC programs. It is because the Lorentz contraction is not so large that the “pancake-shaped disk” approximation used in the original KMW model [2] is no longer valid in these energy regions. Besides, we further extend the formulas of EM fields to incorporate the medium feedback effects according to the Faraday’s induction law, where a constant Ohm conductivity σ_0 is properly and analytically embedded for the pure QGP medium and also a time-dependent conductivity for the realistic QGP evolution. Finally, we make some numerical evaluations of the generalized EM fields formulas in the extended KMW model for the detailed comparisons of time evolution, impact parameter b dependence as well as the prediction of possible lifetime t_{B} of the estimated magnetic field $\mathbf{B}(t, \mathbf{r})$ in comparison with those from the original KMW model.

This paper is organized as follows. We present detailed formulations of the estimated EM fields in the extended KMW model for heavy-ion collisions in Sec. II, which consists of four subparts. We first present in Sec. IIA a formal generalization of the charge distributions from the widely used 3pF model in which the relativistic Lorentz contraction effects on the geometries of both spherically formed and axially deformed colliding nuclei are taken into account. We then in Sec. IIB make a generalization of EM fields in the vacuum starting from the widely used Liénard-Wiechert equations, and naturally generalize the formulas of EM fields with generalized charge distributions and retardation correction. We further extend the EM fields with medium feedback effects by incorporating a constant Ohm electric conductivity σ_0 in Sec. IIC, time-dependent conductivity in Sec. IID and an alternative solution for simulations in APPENDIX A. Some evaluations and comparisons about the time evolution, centrality (impact parameter b) dependence, as well as the prediction of possible lifetime of the estimated magnetic field from the extended KMW model in comparison with those from the original KMW model are presented in Sec. III. We finally summarize the main processes of such generalization along with the conclusions and discussions in Sec. IV. The notation we use in this paper is the rationalized Lorentz-Heaviside units within the natural units, with $\hbar = c = 1$ and $\mu_0 = \epsilon_0 = 1$.

II. ELECTROMAGNETIC FIELDS FROM EXTENDED KMW MODEL

Before the detailed discussion, let us first emphasize that the physical situations of heavy-ion collisions consist of event-by-event \mathcal{P} and \mathcal{CP} violation processes due to the effects of topological charge fluctuation with non-trivial QCD

gauge field configurations (characterized by the topological invariant, the winding number Q_w) in the vicinity of the deconfined QGP phase [2]. This kind of \mathcal{P} and \mathcal{CP} violation processes can only locally happen under some special and even extreme conditions in QCD, such as in the instantaneous deconfined QGP phase with chirality imbalance at extremely high temperature $T \sim \Lambda_{\text{QCD}}$ in the presence of a strong magnetic field $eB \sim m_\pi^2$, which will equivalently generate event-by-event locally non-vanishing θ angle for the effects of so called “ θ -vacuum” [90–92]. In other words, fluctuations of local \mathcal{P} and \mathcal{CP} violated metastable domains of the QCD θ vacuum on the event-by-event basis are intrinsically connected to the amount of charges Q separated by the simultaneous magnetic field \mathbf{B} for the non-trivial gluon field configurations with $Q_w \neq 0$. It means that the expectation value of the amount of separated charges Q is proportional to the strength of magnetic field $|\mathbf{B}|$, hence the charge asymmetry fluctuations $\langle \Delta_\pm^2 \rangle$ will roughly proportional to $|\mathbf{B}|^2$ [2]. It is therefore of crucial importance to quantify the strength of EM fields, especially the time evolution and the possible lifetime t_B of the magnetic field $\mathbf{B}(t, \mathbf{r})$ in relativistic heavy-ion collisions [93, 94].

Similar to the conventional setup of colliding system for heavy-ion collisions, we choose the x axis along the impact parameter b , and z axis along the beam direction of projectile such that the $x - z$ plane is exactly the reaction plane (RP). The y axis is then chosen to be perpendicular to the reaction plane, as illustrated in Fig. 1.

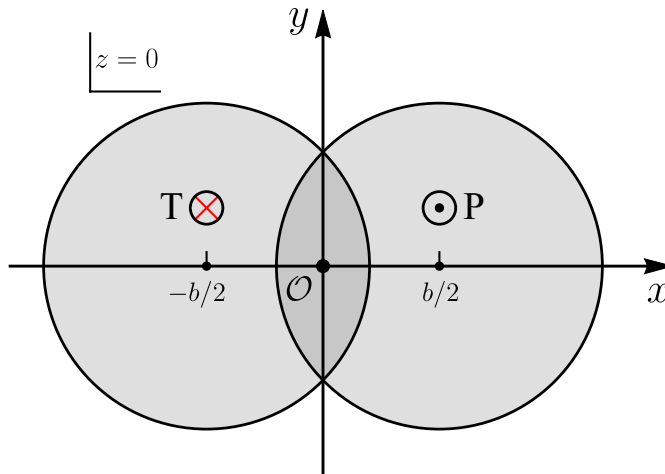


FIG. 1: (Color online) Illustration of the initial geometry of the colliding system projected on the transverse plane ($z = 0$) at an impact parameter b for non-central high-energy nucleus-nucleus collisions. The centers of the projectile (denoted as P) and target (denoted as T) nuclei are respectively located at $(b/2, 0, 0)$ and $(-b/2, 0, 0)$ at $t = 0$ when the two colliding nuclei are completely overlapping with each other, moving parallel or anti-parallel to the beam z direction.

A. Generalization of Charge Distributions for Heavy-ion Collisions

Since in symmetric heavy-ion collisions such as gold-gold collisions at top RHIC energy with the center of mass energy $\sqrt{s} = 200$ GeV per nucleon pair along the z direction, the Lorentz contraction factor $\gamma = \sqrt{s}/(2m_N) \simeq 106.5$ (where m_N is the average nucleon mass), which corresponds to the beam rapidity $Y_0 = \cosh^{-1}(\gamma) \simeq 5.36$. In this case, the two gold nuclei will be Lorentz contracted to be less than 1% of their original size in the z direction, because of which the original KMW model [2] approximates the two colliding nuclei as “pancake-shape disk”. It is further assumed in this model that the charge distribution can be treated as uniformly distributed within the two colliding nuclei and further be limited only within the transverse plane with a two-dimensional surface number density. Therefore in this paper, we will first formulate our generalization of the charge distributions, and hence formulate the estimation of generated EM fields in the extended KMW model.

It has been widely acknowledged that final state anisotropies of emitted charged particles in heavy-ion collisions are very sensitive to the initial conditions, such as the experimentally measured final state charge particle elliptic flow v_2 is actually very sensitive to the initial eccentricity ε_2 [95]. Hence, the initial conditions may dominantly cause the contamination of the experimentally measured CME signal. Therefore, a better quantification of the initial geometry will be of crucial importance, especially for the study of CME in heavy-ion collisions since the initial geometry of charge distributions may significantly modify not only the centrality dependence but also the time evolution of the generated magnetic field $\mathbf{B}(t, \mathbf{r})$.

Besides, due to the relativistic motion of colliding nuclei, the overall size of each nucleus will be Lorentz contracted by a factor of γ along the beam z direction, such that a spherically symmetric nucleus will become an ellipsoidal

nucleus with the volume shrunken by a factor of γ while the charge density magnified by a factor of γ simultaneously. Hence, we first start from generalizing the charge distributions into a relativistic three-dimensional form with the corresponding standard parameters obtained from high-energy electron-scattering measurements [96]. Moreover, what the original high-energy electron-scattering experiments measure is actually the charge spatial distribution in the so-called “Breit Frame” [97] rather than the nuclear density profile with relativistic motion. Hence, we note that the originally inferred charge distribution parameters from electron-scattering experiments should therefore be properly modified [95] so as to be unambiguously implanted into the widely used Monte-Carlo simulations of the initial conditions for the finite-number nucleons sampling of each nucleus [98].

For non-central high-energy nucleus-nucleus (A-A) collisions at center of mass energy $\sqrt{s} = 2\gamma m_N$ per nucleon pair with the same setup of colliding system as illustrated in Fig. 1, the charge distribution used in the original KMW model can be generalized from the widely used charge distribution models listed in [96], e.g. the widely accepted and used three-parameter Fermi model (3pF) for heavy ions, with the relativistic Lorentz contraction effect taken into account. For a source point $\mathbf{r}' = (x', y', z') = (\mathbf{r}'_{\perp}, z')$ within the colliding nucleus (with charge Ze , and $e = |e|$) with its center located at $\mathbf{r}'_c = (0, 0, 0)$, the generalized charge number density reads [27, 96],

$$\rho(\mathbf{r}') = \gamma\rho_0 \frac{1 + \omega [r'/R'(\theta, \phi)]^2}{1 + \exp \{[r' - R'(\theta, \phi)]/d\}} \Theta(\mathbf{r}'), \quad (1)$$

where

$$r' = r'(\gamma) \equiv \sqrt{\mathbf{r}'_{\perp}{}^2 + (\gamma z')^2}. \quad (2)$$

In the expression of $\rho(\mathbf{r}')$ in Eq. (1), the polar and azimuthal angle variations of axially deformed $R'(\theta, \phi)$ is defined as [22, 84, 86]

$$R'(\theta, \phi) = R_0 [1 + \beta_2 Y_2^0(\theta) + \beta_4 Y_4^0(\theta)], \quad (3)$$

where R_0 is the spherical monopole charge radius, $Y_l^m(\theta, \phi)$ denotes the spherical harmonics, with θ being the polar angle with respect to the symmetry axis of each nucleus, and ϕ being the corresponding azimuthal angle, which are respectively defined as $\phi \equiv \sin^{-1}(y'/|\mathbf{r}'_{\perp}|)$ and $\theta \equiv \cos^{-1}(z'/r')$. The diffusion depth of the nuclear surface d can roughly be related to the skin thickness t by $t = 4 \ln(3)d \simeq 4.4d$, where t equals the distance in which the charge density falls from 90% to 10% of its central value ρ_0 .

Note that ω in Eq. (1) is an additional parameter [96], introduced to characterize the charge central depression or elevation phenomena of some nuclide such as ^{40}Ca , relative to the traditional two-parameter Fermi model (2pF) with parameter c (which is in analogue to R' in 3pF model) and d . Only in 3pF model with $\omega = 0$ that the half density radius $R_{1/2} = R'(\theta, \phi)$, which is the distance from the center of the nucleus to the point at which the charge density equals half its central value ρ_0 . ρ_0 is usually regarded as the charge number normalization constant, which can be obtained from the following charge number normalization condition

$$Z = \int_{-R_A}^{+R_A} dx' \int_{-R_A}^{+R_A} dy' \int_{-R_A/\gamma}^{+R_A/\gamma} dz' \rho(\mathbf{r}'). \quad (4)$$

where R_A is the radius of each nucleus. One should note that the γ factor in front of ρ_0 in Eq. (1) is due to the fact that since the volume of each colliding nucleus will be Lorentz contracted by a factor of γ in the z direction, in accordance to which the charge number density will be simultaneously enlarged by a factor of γ at the same time.

The function $\Theta(\mathbf{r}')$ is introduced so as to constrain that the charge density is just within the ellipsoidal colliding nucleus, and it can further be used to separate the spectators from the participants when restricting it just within the transverse plane, namely $\Theta(\mathbf{r}') \rightarrow \tilde{\Theta}(\mathbf{r}'_{\perp})$, which are separately defined as

$$\begin{aligned} \Theta(\mathbf{r}') &= \theta \left[R_A^2 - \mathbf{r}'_{\perp}{}^2 - (\gamma z')^2 \right], \\ \tilde{\Theta}(\mathbf{r}'_{\perp}) &= \theta \left[R_A^2 - \mathbf{r}'_{\perp}{}^2 \right]. \end{aligned} \quad (5)$$

Here we note that $\Theta(\mathbf{r}')$ and $\tilde{\Theta}(\mathbf{r}'_{\perp})$ are similar to the function $\theta(\mathbf{r}'_{\perp})$ introduced in the original KMW model [2]. The function $\theta(x)$ in Eq. (5) is the standard unit step function, which reads

$$\theta(x) = \begin{cases} 0 & x < 0 \\ 1 & x > 0. \end{cases} \quad (6)$$

For a spherically symmetric nucleus ($\beta_2 = \beta_4 = 0$), i.e. the ^{197}Au nucleus, R' is actually independent of polar and azimuthal angle distributions and is just the monopole charge radius, namely $R' = R_0$ (similar to the parameter c in 2pF model), as a consequence of which charge number density $\rho(\mathbf{r}') = \rho(r')$ is only a function of $r'(\gamma)$. In the relativistic situation under this condition, the relativistic three-dimensional density $\rho(\mathbf{r}')$ according to Eq. (1) reads

$$\rho(\mathbf{r}') = \gamma \rho_0 \frac{1 + \omega(r'/R_0)^2}{1 + \exp[(r' - R_0)/d]} \Theta(\mathbf{r}'). \quad (7)$$

However, for an axially deformed nucleus, e.g. the ^{96}Zr nucleus, its shape may deviate from the ideal sphere and the charge distribution will depend on the polar and azimuthal angle distributions, for which Eq. (3) is to some extent introduced so as to account for such kind of charge distribution inside the 3pF model as in Eq. (1). In the characterization of deformations in Eq. (3), $\beta_2 Y_2^0$ and $\beta_4 Y_4^0$ characterize angular variations of $R'(\theta, \phi)$ of quadrupole and hexadecapole deformations respectively, where β_2 and β_4 are the corresponding quadrupole and hexadecapole deformation parameters, and $Y_2^0(\theta)$ and $Y_4^0(\theta)$ are the corresponding spherical harmonics.

B. Electromagnetic Fields from Extended KMW Model in the Vacuum

Since we have generalized the charge number density in a relativistic three-dimensional form in Eq. (1) and Eq. (7), let us now first quote a simple situation where EM fields are generated by a pair of two constantly but oppositely moving point-like charged particles of the same electric charge Ze (where e is the elementary electric charge, $e = |e|$) with rapidity $Y_n = \pm Y$ ($Y > 0$), which corresponds to the velocity $\mathbf{v}_n = (0, 0, \tanh Y_n)$, parallel or anti-parallel to the z direction. We now set that at $t = 0$ the two point-like charged particles are located at $\mathbf{r}'_n(t = 0) = (x'_n, y'_n, z'_n)$. Here the index $n = \pm$ respectively represents the charged particles moving in the positive and negative z -directions. Also, it is worth to note that since in the three-dimensional situation in heavy-ion collisions for a charge point \mathbf{r}'_n within the two colliding nuclei at time $t = 0$ when the two colliding nuclei are usually assumed to be completely overlapping with each other, the z coordinate z'_n for this charge point in general will be non-zero. One can start from using the Liénard-Wiechert (L-W) potentials generated by this two point-like charge particles to evaluate the EM fields for a field point $\mathbf{r} = (x, y, z)$ at observation time t , which gives rise to the following widely used L-W equations of EM fields [3, 5, 8–11, 15, 16, 21–23, 29–34]

$$\begin{aligned} e\mathbf{E}(t, \mathbf{r}) &= \alpha_{\text{EM}} \sum_{n=\pm} Z_n \frac{\mathbf{R}_n (1 - v_n^2)}{\left(R_n^2 - [\mathbf{v}_n \times \mathbf{R}_n]^2\right)^{3/2}}, \\ e\mathbf{B}(t, \mathbf{r}) &= \alpha_{\text{EM}} \sum_{n=\pm} Z_n \frac{\mathbf{v}_n \times \mathbf{R}_n (1 - v_n^2)}{\left(R_n^2 - [\mathbf{v}_n \times \mathbf{R}_n]^2\right)^{3/2}}, \end{aligned} \quad (8)$$

where $\mathbf{R}_n = \mathbf{r} - \mathbf{r}'_n(t)$ are the relative positions of the field point \mathbf{r} to the source points \mathbf{r}'_n at the same observation time t , $\mathbf{r}'_n(t) = (x'_n, y'_n, z'_n) + \mathbf{v}_n t$ are the source positions of the two point-like charge particles at time t , and α_{EM} is the EM fine-structure constant, defined as $\alpha_{\text{EM}} = e^2/4\pi \approx 1/137$. One should note that the retardation effects due to fields propagation have already been incorporated into above equations. For later use convenience, above Eq. (8) can be directly rewritten, in terms of rapidity Y , in the following form,

$$\begin{aligned} e\mathbf{E}(t, \mathbf{r}) &= Z\alpha_{\text{EM}} \sum_{n=\pm} \frac{\cosh(Y_n) \cdot \mathbf{R}_n}{\left\{(x - x'_n)^2 + (y - y'_n)^2 + [t \sinh Y_n - (z - z'_n) \cosh Y_n]^2\right\}^{3/2}}, \\ e\mathbf{B}(t, \mathbf{r}) &= Z\alpha_{\text{EM}} \sum_{n=\pm} \frac{\sinh(Y_n) \cdot \mathbf{e}_z \times \mathbf{R}_n}{\left\{(x - x'_n)^2 + (y - y'_n)^2 + [t \sinh Y_n - (z - z'_n) \cosh Y_n]^2\right\}^{3/2}}, \end{aligned} \quad (9)$$

which in nature are well consistent with the derivation in [2] for the magnetic field generated by a point-like charge when reducing $z'_n \rightarrow 0$ in above Eq. (9). In contrary, $z'_n \neq 0$ is intended for the three-dimensional form of charge distribution such as Eqs. (1) or (7) where the z coordinate of a point-like charge inside the colliding nuclei is not necessarily limited only within the transverse plane, hence we can generalize the “pancake shaped disk” approximation as well as the two-dimensional surface number densities used in the original KMW model [2].

Now one can estimate the strength of EM fields generated in heavy-ion collisions. For a field point $\mathbf{r} = (x, y, z) = (\mathbf{r}_\perp, z)$ at observation time t , the EM fields generated by two identical colliding nuclei with charge Ze and beam

rapidity $\pm Y_0$ ($Y_0 > 0$) parallel or anti-parallel to the z direction can be estimated by combining the generalized relativistic three-dimensional charge number density $\rho(\mathbf{r}')$ in Eq. (1) or Eq. (7) with the EM fields generated by a pair of two point-like charges in Eq. (8) or Eq. (9), and then performing the integration of charge number densities over the corresponding coordinate space within the two colliding nuclei. Nevertheless, the situation will be a little different from the point-like charge case since colliding two heavy ions will separate the charged bulk matter into spectators (denote as S) and participants (denote as P). The participants in general will slow-down to a certain extent due to the baryon-junction stopping effect [99], while the spectators in general are assumed to be moving with the same beam rapidity $Y_b = \pm Y_0$ and do not scatter at all. Therefore, we follow the method proposed in [2] by likewise splitting the contributions to the EM fields generated by the two colliding nuclei into four parts, which simply read as

$$\begin{aligned}\mathbf{E} &= \mathbf{E}_S^+ + \mathbf{E}_S^- + \mathbf{E}_P^+ + \mathbf{E}_P^-, \\ \mathbf{B} &= \mathbf{B}_S^+ + \mathbf{B}_S^- + \mathbf{B}_P^+ + \mathbf{B}_P^-. \end{aligned} \quad (10)$$

For a charge position vector $\mathbf{r}' = (x', y', z') = (\mathbf{r}'_\perp, z')$ with the same setup of colliding system as in Fig. 1, the charge number density $\rho(\mathbf{r}')$ in Eq. (1) or Eq. (7) as well as the corresponding $\Theta(\mathbf{r}')$ and $\tilde{\Theta}(\mathbf{r}'_\perp)$ functions should be accordingly shifted by a half impact parameter vector \mathbf{b} , namely $\rho_\pm(\mathbf{r}') = \rho(\mathbf{r}' \mp \mathbf{b}/2)$, $\Theta_\pm(\mathbf{r}') = \Theta(\mathbf{r}' \mp \mathbf{b}/2)$ and $\tilde{\Theta}_\pm(\mathbf{r}'_\perp) = \tilde{\Theta}(\mathbf{r}'_\perp \mp \mathbf{b}/2)$. The contributions by spectators can therefore be elaborated into the following form

$$\begin{aligned}e\mathbf{E}_S^\pm(t, \mathbf{r}) &= \alpha_{\text{EM}} \cosh(Y_0) \int_{V_\pm} d^3\mathbf{r}' \frac{\rho_\pm(\mathbf{r}') [1 - \tilde{\Theta}_\mp(\mathbf{r}'_\perp)] \mathbf{R}_\pm}{\left\{ (\mathbf{r}_\perp - \mathbf{r}'_\perp)^2 + [t \sinh(\pm Y_0) - (z - z') \cosh Y_0]^2 \right\}^{3/2}}, \\ e\mathbf{B}_S^\pm(t, \mathbf{r}) &= \alpha_{\text{EM}} \sinh(\pm Y_0) \int_{V_\pm} d^3\mathbf{r}' \frac{\rho_\pm(\mathbf{r}') [1 - \tilde{\Theta}_\mp(\mathbf{r}'_\perp)] \mathbf{e}_z \times \mathbf{R}_\pm}{\left\{ (\mathbf{r}_\perp - \mathbf{r}'_\perp)^2 + [t \sinh(\pm Y_0) - (z - z') \cosh Y_0]^2 \right\}^{3/2}}, \end{aligned} \quad (11)$$

where V_\pm donate the ellipsoidal volumes occupied by the two colliding nuclei, which can be related to the integration domains in Eq. (4) for charge number normalization condition.

For EM fields contributed by participants, we at present do not consider contributions by newly created particles either as [2] because the numbers of newly produced positively and negatively charged particles are nearly equal and their expansion is estimated to be almost spherical. Such an assumption should be reasonable, especially for peripheral collisions. Therefore one only needs to take into account the contributions of baryon-junction stopping bulk matter which are initially there. The normalized rapidity Y distributions of the baryon-junction stopping bulk matter of projectile (+) and target (-) can be empirically estimated [2, 17, 28, 99] as

$$f_\pm(Y) = \frac{\alpha_y}{2 \sinh(\alpha_y Y_0)} e^{\pm \alpha_y Y}, \quad -Y_0 \leq Y \leq Y_0. \quad (12)$$

Here we note that the parameter α_y can be estimated as $\alpha_y \simeq \alpha_J^0$, where α_J^0 is the Regge trajectory intercept, defined as $\alpha_J^0(0) \simeq 2\alpha_B(0) - 1 + 3(1 + \alpha_R(0)) \simeq 1/2$ in Regge theory [99–101], in which $\alpha_B(0) \simeq 0$ is the baryon intercept while $\alpha_R(0) \simeq 0.5$ is the Reggeon intercept. Although it has been mentioned early in [101] that a somewhat lower baryon intercept $\alpha_B(0)$ should be used if nucleon exchange effectively dominates, which will somehow give rise to a relatively smaller α_y . Recently, the ALICE Collaboration has reported the data at different center of mass energies \sqrt{s} for the anti-baryons to baryons ratio on baryon stopping [102], which seems to support that $\alpha_y \simeq 0.5$ is experimentally reasonable. Therefore we subjectively to use $\alpha_y \simeq 0.5$ as the principal value in this paper, and also check that varying α_y between 0.48–0.50 does not largely affect the final results for the time evolution of the magnetic field strength.

The contributions to EM fields by participants can therefore be estimated by inserting Eq. (12) into Eq. (9), and then combining with Eqs. (1) or (7), which follow as

$$\begin{aligned}e\mathbf{E}_P^\pm(t, \mathbf{r}) &= \alpha_{\text{EM}} \int_{V_\pm} d^3\mathbf{r}' \int_{-Y_0}^{Y_0} dY \frac{\Psi_\pm(Y) \cosh Y \cdot \rho_\pm(\mathbf{r}') \tilde{\Theta}_\mp(\mathbf{r}'_\perp) \mathbf{R}_\pm}{\left\{ (\mathbf{r}_\perp - \mathbf{r}'_\perp)^2 + [t \sinh Y - (z - z') \cosh Y]^2 \right\}^{3/2}}, \\ e\mathbf{B}_P^\pm(t, \mathbf{r}) &= \alpha_{\text{EM}} \int_{V_\pm} d^3\mathbf{r}' \int_{-Y_0}^{Y_0} dY \frac{\Psi_\pm(Y) \sinh Y \cdot \rho_\pm(\mathbf{r}') \tilde{\Theta}_\mp(\mathbf{r}'_\perp) \mathbf{e}_z \times \mathbf{R}_\pm}{\left\{ (\mathbf{r}_\perp - \mathbf{r}'_\perp)^2 + [t \sinh Y - (z - z') \cosh Y]^2 \right\}^{3/2}}, \end{aligned} \quad (13)$$

where the refined functions $\Psi_\pm(Y)$ for baryon-junction stopping effect are introduced to account for whether the retardation time t_{ret} of a participating charge at observation time t is ahead of the collision time t_c or simply after

the collision time t_c , which reads

$$\Psi_{\pm}(Y) = \theta(t_{\text{ret}} - t_c) f_{\pm}(Y) + \theta(t_c - t_{\text{ret}}) \delta(Y \mp Y_0). \quad (14)$$

Here t_{ret} is obtained by solving the retardation relation $t_{\text{ret}} = t - |\mathbf{r} - \mathbf{r}' - t_{\text{ret}} \cdot \mathbf{e}_z \tanh Y|$ for each rapidity Y within the normalized rapidity integral. We refer to this kind of treatment of participants in Eq. (14) as retardation correction (RC) in this paper. For the case without retardation correction, the functions $\Psi_{\pm}(Y)$ are simply previously used normalized rapidity distribution functions $f_{\pm}(Y)$ in [2, 17, 28], namely $\Psi_{\pm}(Y) = f_{\pm}(Y)$.

The expressions for the estimated EM fields in Eqs. (11) and (13) are in general consistent with the derivation in the original KMW model [2]. One distinct difference is that the depth in the z direction is now taken into account in the extended KMW model rather than the infinitely thin depth (zero z -depth) in the original KMW model, which actually extends the dimensions of the charge density integration. The other distinct difference is that the retardation correction (RC) from the perspective of field propagation for the treatment of participating charges as in Eq. (14) through $\Psi_{\pm}(Y)$ rather than $f_{\pm}(Y)$ in Refs. [2, 17, 28] is now explicitly considered. Hence, we think that our generalization in extended KMW model may give rise to some observable differences for the total estimated EM fields since the retardation due to field propagation is most relevant to the z coordinate. Again, we note that the charge number densities $\rho_{\pm}(\mathbf{r}')$ are not longer the uniformly distributed surface densities, which however are generalized into relativistic 3pF model forms for the incorporation of Lorentz contraction effect and the effect due to deformations with the standard parameters obtained from high-energy electron-scattering measurements [96]. Therefore, Eqs. (11) and (13) will be very easily and appropriately applied to lower energy regions and various colliding systems, where the “pancake-shaped disk” approximation used in the original KMW model [2] is no longer valid.

C. Electromagnetic Fields from Extended KMW Model in the Pure Medium

Up to now, we limit our discussions on the estimated EM fields without considering any medium feedback effects, namely the Ohm electric conductivity $\sigma = \sigma_{\text{Ohm}}$ is vanishing in above discussion for the extended KMW model. For high-temperature ($T \sim \Lambda_{\text{QCD}}$) hot QCD matter, the real QGP is a conducting medium and the electric conductivity σ is generally acknowledged to be proportional to the plasma temperature T [103–109], namely $\sigma \propto T$. Since it is known according to the Faraday’s induction law that the electric conductivity σ may (to some extent) substantially slow down the decrease of the generated EM fields, and therefore largely prolong the lifetime of EM fields, which is verified to be crucial for the estimation of CME in heavy-ion collisions [93, 94]. In order to incorporate the medium feedback effects, we therefore implant a constant electric conductivity σ_0 into the following Maxwell’s equations, which read

$$\begin{aligned} \nabla \cdot \mathbf{E} &= \frac{\rho_{\text{ext}}}{\varepsilon}, \\ \nabla \cdot \mathbf{B} &= 0, \\ \nabla \times \mathbf{E} &= -\partial_t \mathbf{B}, \\ \nabla \times \mathbf{B} &= \partial_t \mathbf{E} + \sigma_0 \mathbf{E} + \mathbf{j}_{\text{ext}}. \end{aligned} \quad (15)$$

We then obtain the following partial differential wave equations for EM fields,

$$\begin{aligned} (\nabla^2 - \partial_t^2 - \sigma_0 \partial_t) \mathbf{B} &= -\nabla \times \mathbf{j}_{\text{ext}}, \\ (\nabla^2 - \partial_t^2 - \sigma_0 \partial_t) \mathbf{E} &= \partial_t \mathbf{j}_{\text{ext}} + \nabla \left(\frac{\rho_{\text{ext}}}{\varepsilon} \right). \end{aligned} \quad (16)$$

The solutions for above EM wave equations have been analytically solved in [24], in which the authors have embedded both electric conductivity σ_0 and chiral magnetic conductivity σ_{χ} for the EM fields generated by a relativistic point-like charge. In the absence of chiral magnetic conductivity σ_{χ} (since in general, $\sigma_{\chi} \ll \sigma_0$), we obtain the following solution in the cylindrical coordinates for the magnetic field generated at a field point $\mathbf{r} = (\mathbf{r}_{\perp}, z) = (x, y, z)$ as

$$\begin{pmatrix} B_r \\ B_{\phi} \\ B_z \end{pmatrix} (t, \mathbf{r}) = \frac{Q}{4\pi} \frac{\gamma v R_{\perp}}{\Delta^{3/2}} \left[1 + \frac{\gamma |v| \sigma_0}{2} \sqrt{\Delta} \right] e^A \begin{pmatrix} 0 \\ 1 \\ 0 \end{pmatrix}, \quad (17)$$

with

$$\begin{aligned} R_{\perp} &\equiv |\mathbf{r}_{\perp} - \mathbf{r}'_{\perp}| = \sqrt{(x - x')^2 + (y - y')^2}, \\ \Delta &\equiv \gamma^2 (vt + z'_0 - z)^2 + R_{\perp}^2, \\ A &\equiv \frac{\gamma v \sigma_0}{2} [\gamma (vt + z'_0 - z)] - \frac{\gamma |v| \sigma_0}{2} \sqrt{\Delta}, \end{aligned} \quad (18)$$

for a point-like charged particle with electric charge $Q = +Ze$ moving with velocity $\mathbf{v} = (0, 0, v)$ along the positive or negative z directions, which is located at $\mathbf{r}' = (\mathbf{r}'_{\perp}, z') = (x', y', z'_0 + vt)$ at observation time t . The radial and longitudinal components of magnetic field B_r and B_z are both vanishing when only the electric conductivity σ_0 is embedded, namely $B_r = B_z = 0$.

The transformations of EM fields \mathbf{F} (where $\mathbf{F} = \mathbf{B}, \mathbf{E}$) in the Cartesian coordinates (F_x, F_y, F_z) with that in the cylindrical coordinates (F_r, F_{ϕ}, F_z) simply read

$$\mathbf{F} = \begin{pmatrix} F_x \\ F_y \\ F_z \end{pmatrix} = \begin{pmatrix} F_r \cos \phi - F_{\phi} \sin \phi \\ F_r \sin \phi + F_{\phi} \cos \phi \\ F_z \end{pmatrix}, \quad (19)$$

where ϕ is the azimuthal angle (with respect to x -axis) of the transverse relative position vector, namely $\mathbf{R}_{\perp} = \mathbf{r}_{\perp} - \mathbf{r}'_{\perp}$. Note that since we have $\mathbf{e}_z \times \mathbf{R} = (y' - y, x - x', 0)$, where $\mathbf{R} = \mathbf{r} - \mathbf{r}'$ is the relative position vector, the magnetic field \mathbf{B} in Eq. (17) in the Cartesian coordinates therefore can be rewritten in a more compact form, which reads

$$\mathbf{B}(t, \mathbf{r}) = \frac{Q}{4\pi} \frac{\gamma v \mathbf{e}_z \times \mathbf{R}}{\Delta^{3/2}} \left[1 + \frac{\gamma |v| \sigma_0}{2} \sqrt{\Delta} \right] e^A, \quad (20)$$

which shares almost the same form as the L-W equation of magnetic field $\mathbf{B}(t, \mathbf{r})$ in Eq. (9) except for the factor $(1 + \gamma |v| \sigma_0 \sqrt{\Delta}/2) e^A$ due to the inclusion of a constant electric conductivity σ_0 for the QGP medium response. Therefore, Eq. (20) can naturally reproduce the well-known L-W equation of magnetic field in the vacuum, i.e., Eq. (8) or Eq. (9), when the electric conductivity σ_0 is vanishing. For a special situation in Eq. (17) when the azimuthal angle $\phi = 0$, the x component of magnetic field B_x is consequently vanishing and the tangential ϕ component of magnetic field B_{ϕ} is actually B_y and along the y direction, as is usually mentioned in literature [14]. Also, we note that the expression of \mathbf{B} in Eq. (17) was firstly derived in Ref. [14, 17].

For the electric field \mathbf{E} , the tangential component of electric field E_{ϕ} can be easily obtained by applying the relation $E_{\phi} = -v B_r = 0$. Meanwhile, the authors in [24] have obtained the following explicit expressions for both radial and longitudinal components E_r and E_z in the leading linear order of σ_0 for high-energy heavy-ion collisions as

$$\begin{aligned} E_r(t, \mathbf{r}) &= \frac{Q}{4\pi} \left\{ \frac{\gamma R_{\perp}}{\Delta^{3/2}} \left(1 + \frac{\gamma |v| \sigma_0}{2} \sqrt{\Delta} \right) - \frac{\sigma_0}{|v| R_{\perp}} \left[1 + \frac{\gamma |v|}{\sqrt{\Delta}} \left(t - \frac{z - z'_0}{v} \right) \right] e^{-\sigma_0 [t - (z - z'_0)/v]} \right\} e^A, \\ E_{\phi}(t, \mathbf{r}) &= 0, \\ E_z(t, \mathbf{r}) &= \frac{Q}{4\pi} \left\{ \frac{\sigma_0^2 v}{|v|^3} e^{-\sigma_0 [t - (z - z'_0)/v]} \Gamma(0, -A) + \frac{e^A}{\Delta^{3/2}} \left[\gamma(z - z'_0 - vt) - \frac{v}{|v|} A \sqrt{\Delta} - \frac{\gamma v \sigma_0}{v^2} \Delta \right] \right\}, \end{aligned} \quad (21)$$

where $\Gamma(0, -A) = \int_{-A}^{\infty} dt \exp(-t)/t$ is the incomplete gamma function. According to the transformations in Eq. (19), the radial and longitudinal components of electric field E_r and E_z are respectively along the x and z directions when the azimuthal angle $\phi = 0$. Here we note that Eqs. (17) and (21) can naturally reduce to the well-known L-W equations of EM fields in the vacuum when the electric conductivity σ_0 is vanishing ($\sigma_0 = 0$). It has been further proved in [24] that Eqs. (17) and (21) are self-consistent and well satisfy the Maxwell's equations in Eq. (15). Hence in the following, we will generalize above EM fields for point-like charge in Eqs. (17) and (21), and make them more applicable for high-energy nucleus-nucleus collisions.

We then combine the electric conductivity σ_0 embedded EM fields in Eqs. (17) and (21) with the relativistic three-dimensional charge number density in Eq. (1) or Eq. (7), and then apply the decomposition of EM fields as in Eq. (10). In analogue to Eqs. (11) and (13), we finally obtain the following explicit expressions of the magnetic field embedded with a constant electric conductivity σ_0 . For the contributions of spectators, we obtain

$$e\mathbf{B}_S^{\pm}(t, \mathbf{r}) = \lim_{Y \rightarrow \pm Y_0} \alpha_{\text{EM}} \sinh Y \int_{V_{\pm}} d^3 \mathbf{r}' \frac{\rho_{\pm}(\mathbf{r}') \left[1 - \tilde{\Theta}_{\mp}(\mathbf{r}'_{\perp}) \right] \mathbf{e}_z \times \mathbf{R}_{\pm}}{\Delta^{3/2}} \left[1 + \frac{\sigma_0 \sinh |Y|}{2} \sqrt{\Delta} \right] e^A, \quad (22)$$

with the definitions in Eq. (18) accordingly rewritten as

$$\begin{aligned} R_{\perp} &\equiv |\mathbf{r}_{\perp} - \mathbf{r}'_{\perp}| = \sqrt{(x - x')^2 + (y - y')^2}, \\ \Delta &\equiv [t \sinh Y - (z - z') \cosh Y]^2 + R_{\perp}^2, \\ A &\equiv \frac{\sigma_0 \sinh Y}{2} [t \sinh Y - (z - z') \cosh Y] - \frac{\sigma_0 \sinh |Y|}{2} \sqrt{\Delta}, \end{aligned} \quad (23)$$

where $\mathbf{R}_\pm = \mathbf{r} - \mathbf{r}'(t)$ are the relative positions of the field point \mathbf{r} to the source point \mathbf{r}' at the observation time t . Again, the positive and negative signs \pm correspond to the nuclei moving in the positive and negative z -directions. For the contributions of participants, we have

$$e\mathbf{B}_P^\pm(t, \mathbf{r}) = \alpha_{\text{EM}} \int_{V_\pm} d^3\mathbf{r}' \int_{-Y_0}^{Y_0} dY \frac{\Psi_\pm(Y) \sinh Y \cdot \rho_\pm(\mathbf{r}') \tilde{\Theta}_\mp(\mathbf{r}'_\perp) \mathbf{e}_z \times \mathbf{R}_\pm}{\Delta^{3/2}} \left[1 + \frac{\sigma_0 \sinh |Y|}{2} \sqrt{\Delta} \right] e^A. \quad (24)$$

For the electric field \mathbf{E} generated by two colliding nuclei, we first notice that E_ϕ is vanishing in the point-like charge case, therefore there is no contribution from both spectators and participants for the tangential component electric field E_ϕ . The cylindrical coordinates are usually not extensively used in heavy-ion collisions, we therefore directly transform the expressions of electric field in the Cartesian coordinates after invoking Eq. (19) as follows,

$$\begin{aligned} \begin{pmatrix} eE_{x,S}^\pm \\ eE_{y,S}^\pm \end{pmatrix} (t, \mathbf{r}) &= \lim_{Y \rightarrow \pm Y_0} \alpha_{\text{EM}} \int_{V_\pm} d^3\mathbf{r}' \rho_\pm(\mathbf{r}') \left[1 - \tilde{\Theta}_\mp(\mathbf{r}'_\perp) \right] \left\{ \frac{R_\perp \cosh Y}{\Delta^{3/2}} \left(1 + \frac{\sigma_0 \sinh |Y|}{2} \sqrt{\Delta} \right) \right. \\ &\quad \left. - \frac{\sigma_0}{R_\perp \tanh |Y|} \left[1 + \frac{\sinh |Y|}{\sqrt{\Delta}} \left(t - \frac{z - z'}{\tanh Y} \right) \right] \exp \left(-\sigma_0 \left[t - \frac{z - z'}{\tanh Y} \right] \right) \right\} \frac{e^A}{R_\perp} \begin{pmatrix} x - x' \\ y - y' \end{pmatrix}, \\ \begin{pmatrix} eE_{x,P}^\pm \\ eE_{y,P}^\pm \end{pmatrix} (t, \mathbf{r}) &= \alpha_{\text{EM}} \int_{V_\pm} d^3\mathbf{r}' \int_{-Y_0}^{Y_0} dY \Psi_\pm(Y) \rho_\pm(\mathbf{r}') \tilde{\Theta}_\mp(\mathbf{r}'_\perp) \left\{ \frac{R_\perp \cosh Y}{\Delta^{3/2}} \left(1 + \frac{\sigma_0 \sinh |Y|}{2} \sqrt{\Delta} \right) \right. \\ &\quad \left. - \frac{\sigma_0}{R_\perp \tanh |Y|} \left[1 + \frac{\sinh |Y|}{\sqrt{\Delta}} \left(t - \frac{z - z'}{\tanh Y} \right) \right] \exp \left(-\sigma_0 \left[t - \frac{z - z'}{\tanh Y} \right] \right) \right\} \frac{e^A}{R_\perp} \begin{pmatrix} x - x' \\ y - y' \end{pmatrix}, \end{aligned} \quad (25)$$

which are respectively the contributions of spectators and participants for the x and y components of electric field E_x and E_y . For the z component of electric field E_z contributed by spectators and participants, we have

$$\begin{aligned} eE_{z,S}^\pm(t, \mathbf{r}) &= \lim_{Y \rightarrow \pm Y_0} \alpha_{\text{EM}} \int_{V_\pm} d^3\mathbf{r}' \rho_\pm(\mathbf{r}') \left[1 - \tilde{\Theta}_\mp(\mathbf{r}'_\perp) \right] \left\{ \frac{\text{sgn}(Y) \sigma_0^2}{\tanh^2 Y} \exp \left(-\sigma_0 \left[t - \frac{z - z'}{\tanh Y} \right] \right) \Gamma(0, -A) \right. \\ &\quad \left. + \frac{e^A}{\Delta^{3/2}} \left[(z - z') \cosh Y - t \sinh Y - \text{sgn}(Y) A \sqrt{\Delta} - \frac{\sigma_0 \sinh Y}{\tanh^2 Y} \Delta \right] \right\}, \\ eE_{z,P}^\pm(t, \mathbf{r}) &= \alpha_{\text{EM}} \int_{V_\pm} d^3\mathbf{r}' \int_{-Y_0}^{Y_0} dY \Psi_\pm(Y) \rho_\pm(\mathbf{r}') \tilde{\Theta}_\mp(\mathbf{r}'_\perp) \left\{ \frac{\text{sgn}(Y) \sigma_0^2}{\tanh^2 Y} \exp \left(-\sigma_0 \left[t - \frac{z - z'}{\tanh Y} \right] \right) \Gamma(0, -A) \right. \\ &\quad \left. + \frac{e^A}{\Delta^{3/2}} \left[(z - z') \cosh Y - t \sinh Y - \text{sgn}(Y) A \sqrt{\Delta} - \frac{\sigma_0 \sinh Y}{\tanh^2 Y} \Delta \right] \right\}, \end{aligned} \quad (26)$$

where the sign function $\text{sgn}(Y) = Y/|Y|$ denotes the sign of rapidity Y . Note that Eqs. (22-26) quantify the x , y and z components of EM fields contributed by spectators and participants in heavy-ion collisions with a constant electric conductivity σ_0 implemented, where we also incorporate the generalized relativistic charge distributions, e.g., the 3pF model in Eqs. (1) or (7), and the retardation correction (RC) through $\Psi_\pm(Y)$. On the one hand, we currently in Eqs. (22-26) do not include the chiral magnetic conductivity σ_χ into the Maxwell's equations in Eq. (15) since in general $\sigma_\chi \ll \sigma$. Also, the value of electric conductivity σ from recent lattice calculations [103–109] still shows very large uncertainties, which may easily submerge the contributions from chiral magnetic conductivity σ_χ . On the other hand, as has shown in [24] that even when the chiral magnetic conductivity σ_χ is included, the dominative components such as B_ϕ , E_r and E_z will not be changed at all. Therefore, we hold the point of view that Eqs. (22-26) can well quantify the dominant contributions of medium feedback effects for the time evolution and centrality (impact parameter b) dependence of EM fields generated in heavy-ion collisions.

Here we note that the chiral magnetic conductivity σ_χ in general will be complex due to the spatially anti-symmetric part of the off diagonal photon polarization tensor, as has been formally discussed and evaluated in [45] by using the linear response theory. It has also been shown in [45] that the chiral magnetic conductivity σ_χ has very strong frequency ω and temperature T dependence, and the induced current $j(t)$ can even change from positive to negative in the time evolution. We therefore currently postpone the inclusion of the chiral magnetic conductivity σ_χ into the extended KMW model, but leave it to our future study.

D. Electromagnetic Fields from Extended KMW Model during the QGP Evolution

It is generally acknowledged in the field of heavy-ion collisions that the QGP can be created at the condition of high collision energies, extremely high temperatures and large energy densities. Such a condition should be satisfied

in Au+Au collisions at $\sqrt{s} = 200$ GeV at RHIC or in Pb+Pb collisions at $\sqrt{s} = 2760$ GeV at LHC. These created deconfined QCD matter can only exist after heavy-ion collisions. Thus, the conducting property of the medium should only exist after the medium time t_σ ($t_\sigma \gtrsim 0$), which is the time that we assume the medium feedback effects start to work.

In such a sense as we mention above, medium feedback effects should only be considered when the retardation time t_{ret} is after the medium time t_σ , ahead of which one should consider using the formulas of EM fields in the vacuum. When the conductivity σ is switched on after the medium time t_σ , one can roughly approximate the medium effects by using a constant Ohm electric conductivity σ_0 for simplicity. Hence, a time-dependent step-function-like conductivity could be employed, namely $\sigma \rightarrow \tilde{\sigma} = \sigma_0 \cdot \theta(t_{\text{ret}} - t_\sigma)$. Thus for the generated magnetic field, Eqs. (22-24) should be accordingly modified as follows

$$e\mathbf{B}_S^\pm(t, \mathbf{r}) = \lim_{Y \rightarrow \pm Y_0} \alpha_{\text{EM}} \sinh Y \int_{V_\pm} d^3\mathbf{r}' \frac{\rho_\pm(\mathbf{r}') [1 - \tilde{\Theta}_\mp(\mathbf{r}'_\perp)] \mathbf{e}_z \times \mathbf{R}_\pm}{\Delta^{3/2}} \left[1 + \frac{\tilde{\sigma} \sinh |Y|}{2} \sqrt{\Delta} \right] e^{\tilde{A}}, \quad (27)$$

$$e\mathbf{B}_P^\pm(t, \mathbf{r}) = \alpha_{\text{EM}} \int_{V_\pm} d^3\mathbf{r}' \int_{-Y_0}^{Y_0} dY \frac{\Psi_\pm(Y) \sinh Y \cdot \rho_\pm(\mathbf{r}') \tilde{\Theta}_\mp(\mathbf{r}'_\perp) \mathbf{e}_z \times \mathbf{R}_\pm}{\Delta^{3/2}} \left[1 + \frac{\tilde{\sigma} \sinh |Y|}{2} \sqrt{\Delta} \right] e^{\tilde{A}}, \quad (28)$$

for the contributions of spectators and participants, with

$$\begin{aligned} R_\perp &\equiv |\mathbf{r}_\perp - \mathbf{r}'_\perp| = \sqrt{(x - x')^2 + (y - y')^2}, \\ \Delta &\equiv [t \sinh Y - (z - z') \cosh Y]^2 + R_\perp^2, \\ \tilde{A} &\equiv \frac{\sinh Y}{2} [t \sinh Y - (z - z') \cosh Y] - \frac{\tilde{\sigma} \sinh |Y|}{2} \sqrt{\Delta}. \end{aligned} \quad (29)$$

Likewise, the generated electric field in Eqs. (30-31) should be modified as

$$\begin{aligned} \begin{pmatrix} eE_{x,S}^\pm \\ eE_{y,S}^\pm \end{pmatrix} (t, \mathbf{r}) &= \lim_{Y \rightarrow \pm Y_0} \alpha_{\text{EM}} \int_{V_\pm} d^3\mathbf{r}' \rho_\pm(\mathbf{r}') [1 - \tilde{\Theta}_\mp(\mathbf{r}'_\perp)] \left\{ \frac{R_\perp \cosh Y}{\Delta^{3/2}} \left(1 + \frac{\tilde{\sigma} \sinh |Y|}{2} \sqrt{\Delta} \right) \right. \\ &\quad \left. - \frac{\tilde{\sigma}}{R_\perp \tanh |Y|} \left[1 + \frac{\sinh |Y|}{\sqrt{\Delta}} \left(t - \frac{z - z'}{\tanh Y} \right) \right] \exp \left(-\tilde{\sigma} \left[t - \frac{z - z'}{\tanh Y} \right] \right) \right\} \frac{e^{\tilde{A}}}{R_\perp} \begin{pmatrix} x - x' \\ y - y' \end{pmatrix}, \\ \begin{pmatrix} eE_{x,P}^\pm \\ eE_{y,P}^\pm \end{pmatrix} (t, \mathbf{r}) &= \alpha_{\text{EM}} \int_{V_\pm} d^3\mathbf{r}' \int_{-Y_0}^{Y_0} dY \Psi_\pm(Y) \rho_\pm(\mathbf{r}') \tilde{\Theta}_\mp(\mathbf{r}'_\perp) \left\{ \frac{R_\perp \cosh Y}{\Delta^{3/2}} \left(1 + \frac{\tilde{\sigma} \sinh |Y|}{2} \sqrt{\Delta} \right) \right. \\ &\quad \left. - \frac{\tilde{\sigma}}{R_\perp \tanh |Y|} \left[1 + \frac{\sinh |Y|}{\sqrt{\Delta}} \left(t - \frac{z - z'}{\tanh Y} \right) \right] \exp \left(-\tilde{\sigma} \left[t - \frac{z - z'}{\tanh Y} \right] \right) \right\} \frac{e^{\tilde{A}}}{R_\perp} \begin{pmatrix} x - x' \\ y - y' \end{pmatrix}, \end{aligned} \quad (30)$$

for the x and y components of contributions from spectators and participants. For that of z components, we have

$$\begin{aligned} eE_{z,S}^\pm(t, \mathbf{r}) &= \lim_{Y \rightarrow \pm Y_0} \alpha_{\text{EM}} \int_{V_\pm} d^3\mathbf{r}' \rho_\pm(\mathbf{r}') [1 - \tilde{\Theta}_\mp(\mathbf{r}'_\perp)] \left\{ \frac{\text{sgn}(Y) \tilde{\sigma}^2}{\tanh^2 Y} \exp \left(-\tilde{\sigma} \left[t - \frac{z - z'}{\tanh Y} \right] \right) \Gamma(0, -\tilde{A}) \right. \\ &\quad \left. + \frac{e^{\tilde{A}}}{\Delta^{3/2}} \left[(z - z') \cosh Y - t \sinh Y - \text{sgn}(Y) \tilde{A} \sqrt{\Delta} - \frac{\tilde{\sigma} \sinh Y}{\tanh^2 Y} \Delta \right] \right\}, \\ eE_{z,P}^\pm(t, \mathbf{r}) &= \alpha_{\text{EM}} \int_{V_\pm} d^3\mathbf{r}' \int_{-Y_0}^{Y_0} dY \Psi_\pm(Y) \rho_\pm(\mathbf{r}') \tilde{\Theta}_\mp(\mathbf{r}'_\perp) \left\{ \frac{\text{sgn}(Y) \tilde{\sigma}^2}{\tanh^2 Y} \exp \left(-\tilde{\sigma} \left[t - \frac{z - z'}{\tanh Y} \right] \right) \Gamma(0, -\tilde{A}) \right. \\ &\quad \left. + \frac{e^{\tilde{A}}}{\Delta^{3/2}} \left[(z - z') \cosh Y - t \sinh Y - \text{sgn}(Y) \tilde{A} \sqrt{\Delta} - \frac{\tilde{\sigma} \sinh Y}{\tanh^2 Y} \Delta \right] \right\}. \end{aligned} \quad (31)$$

Here we note that when the retardation time t_{ret} is ahead of the medium time t_σ , namely $t_{\text{ret}} < t_\sigma$, the conductivity $\tilde{\sigma}$ will vanish and Eqs. (27-31) will naturally reduce to the formulas of EM fields in the vacuum, i.e. Eqs. (10-14). Such a consistent property has been clearly revealed in the point-like charge case, see Eqs. (20-21). Thus we would like to refer to Eqs. (27-31) as a simplified, “mixed” estimation of generated EM fields with contributions from both source charges in the vacuum and source charges in the medium. In the same sense, we can refer to Eqs. (22-26) as the estimation of EM fields in the pure medium, and Eqs. (20-21) as the one in the pure vacuum.

Before we move forward, let us make some short remarks here. The merits of above generalization for the charge number densities as well as the formulations of estimated EM fields both in the pure vacuum in Eqs. (10-14), in the pure medium in Eqs. (22-26) and in the realistic QGP medium in Eqs. (27-31) in the extended KMW model can be at least boiled down to two points: one is that it is more realistically akin to the physical situations for charge distributions with relativistic motion, for which both spherical formed and axially deformed charge number densities are explicitly elaborated, e.g., Eqs. (1) or (7). Therefore, the formulations of estimated EM fields based on the generalized charge number densities can be easily applied to various colliding systems, such as the asymmetric Cu + Au colliding system or the ongoing STAR experiments of isobar colliding systems in which the ^{96}Zr and ^{96}Ru nuclei are widely regarded as an axially deformed nucleus [84–87]. Here we note that a lot of discussions and the related estimations for the EM fields generated in isobar collisions have been presented [31, 33, 84, 86, 88, 89, 110].

Meanwhile, since the charge number density $\rho(\mathbf{r}')$ in Eqs. (1) or (7) is formally embedded with relativistic effect due to Lorentz contraction, it will be much more appropriate and adaptable for the situation at very low energy region when the Lorentz contraction effect is not that significantly large, such as at the lower RHIC energy with $\sqrt{s} = 7.7 \text{ GeV}$ where the Lorentz factor $\gamma \sim 4$. As a comparison, the “pancake shape disk” approximation used in [2] will only be a good approximation in high energy region where the Lorentz factor γ is substantially large. Therefore the model proposed in this paper will be much more appropriate for applications to the STAR-BES program, and some even lower energy region like the under planning FAIR, NICA and J-PARC programs.

The other point is that since the estimation of generated EM fields are explicitly embedded with medium feedback effects through a constant electric conductivity σ_0 in the pure QGP medium and the time-dependent conductivity $\tilde{\sigma}(t)$ in the realistic QGP medium, along with the refined baryon-junction stopping effect with proper retardation correction in Eq. (14), the generalized formulas of EM fields from Eqs. (10-14) in the pure vacuum, or Eqs. (22-26) in the pure medium and Eqs. (27-31) in the realistic QGP evolution hence can further be used for many EM fields related studies, such as the CME related charge asymmetry fluctuations like a_{++} or a_{+-} correlators [2, 68, 87, 110], CME current $\mathbf{J}_\chi = \sigma_\chi \mathbf{B}$ and its related studies for chiral magnetic conductivity σ_χ [45], the in-medium particle’s mass [54–60] as well as QCD phase diagram under strong magnetic field [62–65], and so on.

III. RESULTS AND DISCUSSIONS

Since we have explicitly formulated the estimations of generated EM fields for heavy-ion collisions in the vacuum in Eqs. (10-14), in the pure QGP medium in Eqs. (22-26) and during the realistic QGP evolution in Eqs. (27-31), as well as an alternative solution to the currently used Monte-Carlo simulations of point-like charges in the medium in Eqs. (A.1-A.3), let us first give some pre-analysis before performing the *ab initio* integration of charge distribution or event-by-event simulations of generated EM fields at specific space-time points. Due to the mirror and centrosymmetric symmetries of the colliding system (as is illustrated in Fig. 1), the total electric field \mathbf{E} will vanish while the total magnetic field \mathbf{B} will only remain its y component pointing in the negative y direction at the center point $\mathbf{r} = \mathbf{0}$ of the overlapping region, which further results in a charge separation due to the CME. Therefore, we mainly focus on the y component of magnetic field B_y in this paper.

Let us first declare some abbreviations that we will present in the following. The original KMW model is incorporated with a two-dimensional (2D) surface charge number density, which is abbreviated as 2D KMW. The extended KMW model is generalized with three-dimensional (3D) volume charge number density, which is likewise abbreviated as 3D KMW including two cases: with (w/) and without (w/o) retardation correction (RC). The pure vacuum case and pure medium case is abbreviated as “Pure Vac.” and “Pure Med.”, such that the case during the realistic QGP evolution in Eqs. (27-31) is abbreviated as “Mixed”. The collision time t_c and medium time t_σ for simplicity are chosen at fully overlapping time, namely $t_c = t_\sigma = 0$. Besides, we do check that even when one considers the collision time t_c in Eq. (14) totally from the geometry consideration regardless of the causality reason according to the theory of special relativity, namely the collision time t_c is estimated as $t_c = -t_d$, where t_d is the departure time defined in following Eq. (32), our results basically will not be changed due to the much earlier retardation time t_{ret} .

It should also be noted that the formulation of estimated magnetic field in the original KMW model is actually only limited in the vacuum case without considering medium effects. In order to make a better comparison in the pure conducting medium, we also show the generalized 2D KMW model embedded with a constant electric conductivity σ_0 , which can be easily obtained from the reduction of extended KMW model by removing the longitudinal position dependence and replacing the corresponding charge number density ρ . Such a generalization of magnetic field in the pure conducting medium is actually consistent with that in Refs. [17, 28].

Moreover, it is mainly the magnetic field strength that has been numerically evaluated in the original KMW model [2], and also the following papers [17, 28]. For the sake of comparison, we only show the results of estimated magnetic field in this paper. The results of estimated electric field can be similarly estimated from the extended KMW model in the same way as we present here.

A. Time Evolution of the Magnetic Field Strength

Let us now make a sample comparison of the time evolution of the total magnetic field strength estimated from Eq. (10) in the vacuum. In Fig. 2, we show the estimation of time evolution of the total magnetic field strength $e\mathbf{B}(t, \mathbf{r})$ in the vacuum at the center point $\mathbf{r} = \mathbf{0}$ of the overlapping region in Au+Au collisions at $\sqrt{s} = 200$ GeV with different impact parameters ($b = 4, 8, 12$ fm). From the inserted plot in the upper panel, one can clearly see that the magnetic field from the 3D KMW model with and without retardation correction at $t = 0$ will systematically yield a relatively smaller magnetic field strength (especially for larger impact parameter b), compared with that too sharp cusp of magnetic field strength around $t \sim 0$ from the original KMW model. It can intuitively attributed to the more localized and central elevated charge distribution used in the original KMW model. We check that our results at $t = 0$ are actually consistent with the numerical simulations from HIJING model in [10], which will be clearly redemonstrated in the next subsection.

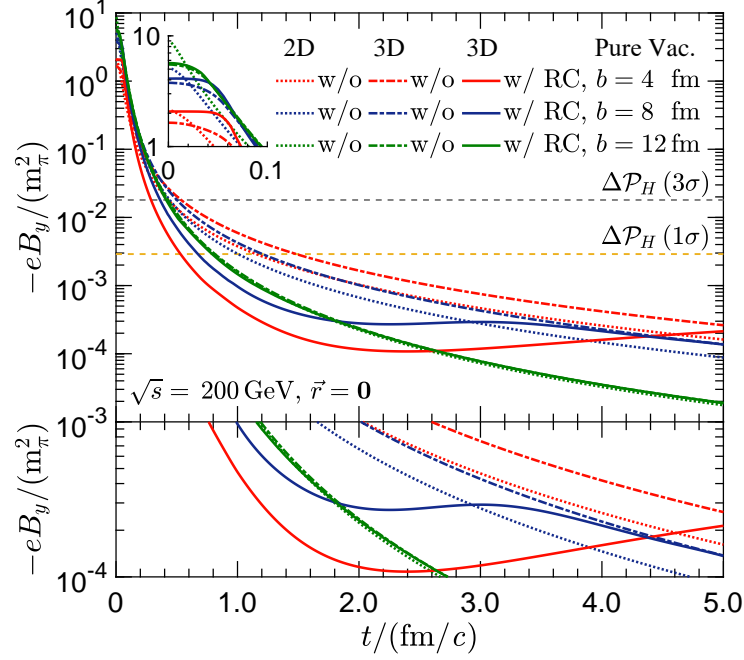


FIG. 2: (Color online) Comparison of the time evolution of the total magnetic field strength in the pure vacuum from extended KMW model with (w/) and without (w/o) retardation correction (RC) and that from original KMW model at different impact parameters $b = 4, 8, 12$ fm for the center point $\mathbf{r} = \mathbf{0}$ of the overlapping region in Au+Au collisions at $\sqrt{s} = 200$ GeV. The two dashed horizontal lines indicate the later-time constraints of the magnetic field strength estimated in [94] from the difference between global polarizations of Λ and $\bar{\Lambda}$ hyperons in Au+Au collisions at $\sqrt{s} = 200$ GeV in [112] at one standard deviation (1σ) and three standard deviations (3σ), respectively.

However, compared with that “seemingly enhanced” magnetic field strength from the extended KMW model without retardation correction, it is also noticeable that the original KMW model will generally give rise to a weaker magnetic field strength just shortly ($t \sim 0.03$ fm/c) after the collision, and the differences in between become rather noticeable at later times for more central (or smaller impact parameter b) collisions. Thus the extended KMW model without retardation correction will yield a longer lifetime t_B of the magnetic field than the original KMW model. When incorporated with retardation correction, however, the magnetic field strength from the extended KMW model will firstly decrease very fast, and then decrease slowly and even grow up to a certain extent for some time range at some impact parameters, e.g., $b = 4, 8$ fm, as clearly shown in the lower panel of Fig. 2. This can be intuitively understood as follows: when incorporated with the retardation correction in Eq. (14), the baryon-junction stopping effects represented through $f_{\pm}(Y)$ in Eq. (14) are basically ruled out by the $\theta(t_{\text{ret}} - t_c)$ function during the comparison of retardation time t_{ret} with the collision time t_c . The contributions from charged participants are mainly dominated by those with beam rapidity $\pm Y_0$, hence the magnetic field strength at early stage decreases much faster than those without retardation correction; At middle or later stage time evolution, however, the contribution from baryon-junction stopping bulk matter grows dominant since the spectators have flown away. The resulting magnetic field strength contributed by those participants will increase first and then decrease. Hence the resulting total magnetic field strength will show non-monotonic behaviors, especially for smaller impact parameter b due to larger baryon-

junction stopping bulk matter. This can be interpreted as a result of the competition between retardation effect of field propagation and baryon-junction stopping effect of participants.

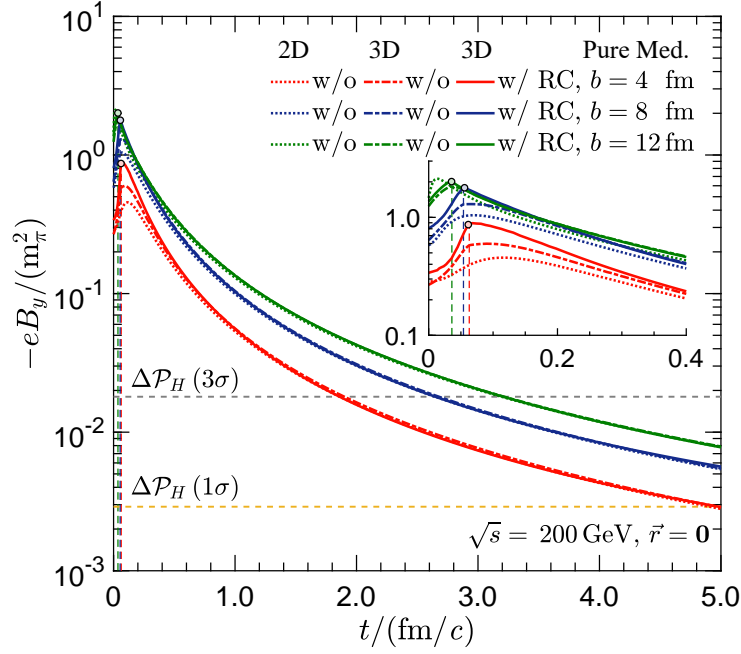


FIG. 3: (Color online) Comparison of the time evolution of the total magnetic field strength in the pure medium with constant Ohm electric conductivity $\sigma_0 = 5.8 \text{ MeV}$ from extended KMW model with (w/) and without (w/o) retardation correction (RC) and that from generalized original KMW model at different impact parameters $b = 4, 8, 12 \text{ fm}$ for the center point $\mathbf{r} = \mathbf{0}$ of the overlapping region in Au+Au collisions at $\sqrt{s} = 200 \text{ GeV}$. The two dashed horizontal lines indicate the later-time constraints of the magnetic field strength estimated in [94] from the difference between global polarizations of Λ and $\bar{\Lambda}$ hyperons in Au+Au collisions at $\sqrt{s} = 200 \text{ GeV}$ in [112] at one standard deviation (1σ) and three standard deviations (3σ), respectively.

The electric conductivity σ_0 has been calculated by using a first principal lattice QCD approach in the quenched approximation in Ref. [106], according to which we set the electric conductivity $\sigma_0 = 5.8 \text{ MeV}$ in this paper so as to make estimations of the magnetic field generated in the conducting QGP medium. In Fig. 3, we show the estimations of time evolution of the magnetic field strength in the pure conducting medium with $\sigma_0 = 5.8 \text{ MeV}$ from the extended KMW model with and without retardation correction and that from the original KMW model at the center point $\mathbf{r} = \mathbf{0}$ of the overlapping region in Au+Au collisions at $\sqrt{s} = 200 \text{ GeV}$ with different impact parameters $b = 4, 8, 12 \text{ fm}$. One can clearly see that the magnetic field strength in the pure conducting QGP medium case in Fig. 3 decays much slower than that in the vacuum case in Fig. 2. There clearly show non-monotonic behaviors of the magnetic field strength at early-time stages for different impact parameters in the pure conducting QGP medium rather than the monotonically decreasing behaviors of magnetic field strength in the vacuum. Besides, compared with the original KMW model, we find the extended KMW model will in general systematically yield a relatively larger magnetic field strength in the conducting QGP medium except at very early stage around $t \sim 0$. Also, we notice that the differences between any two cases become more significant around the non-monotonic peaks ($t \sim 0.1 \text{ fm/c}$), especially for smaller impact parameter b .

Moreover, we notice that the time evolution of the estimated magnetic field strength in the pure conducting medium at later-time stages evolution in Fig. 3 is quite different from that in the vacuum case in Fig. 2 for the impact parameter b dependence. This can be intuitively understood as follows: since in the vacuum case there is no medium feedback effect due to the vanishing electric conductivity, the magnetic field decays quickly and there is only the baryon-junction stopping effect that may to some extent hinder the moving charged bulk matter from flying away from the field point $\mathbf{r} = \mathbf{0}$. Thus the baryon-junction stopping effect will dominate in the later stage of time evolution especially for smaller impact parameter b due to larger charged bulk matter of participants, the resulting total magnetic field strength therefore becomes larger for smaller impact parameter b at later time stage. In the pure conducting medium, however, since the electric conductivity σ_0 is always constant and non-negligible, it is the Faraday's induction effect rather than the baryon-junction stopping effect that dominates for the later time evolution. The resulting total magnetic field strength in the pure conducting medium therefore shows rather distinct impact parameter b dependence at later time stage. In the pure conducting medium, we also notice that the original

KMW model and the extended KMW model can give almost identical results after $t \gtrsim 1.0 \text{ fm}/c$, and the difference in between grows smaller during the time evolution which is quite different from that in the pure vacuum case.

The “kinks” marked as the points at different impact parameters b for the extended KMW model in Fig. 3 are due to the fact that the two colliding nuclei start to separate from each other. The corresponding vertical lines indicate the departure time t_d when the two colliding nuclei just depart from each other, which can be estimated from the following geometry relation in the $x - z$ plane (RP) at an impact parameter b as follows

$$t_d = t_d(b) \equiv \frac{R_A}{\gamma} \sqrt{1 - \left(\frac{b}{2R_A}\right)^2}. \quad (32)$$

The original KMW model due to the same reason actually also have “kinks”, which however are all located at $t = 0$ (we do not show in Fig. 3), since the charges in the original KMW model are restricted within the transverse plane with zero depth in the z direction.

By using the interesting idea proposed in the recent Ref. [94], one can use the experimentally measured polarization data [111, 112] on Λ and $\bar{\Lambda}$ hyperons to make some rough constraints on the allowed later-time magnetic field strength, which has also been recently explored in Ref. [113]. It has been estimated in [94] that in the one standard deviation (1σ) limit of the recent measurements on global polarization of Λ and $\bar{\Lambda}$ hyperons in Au+Au collisions at $\sqrt{s} = 200 \text{ GeV}$ [112], the magnetic field strength at thermal freeze-out time can be estimated as

$$e|B| = \frac{eT_s |\Delta \mathcal{P}_H|}{2|\mu_\Lambda|} < 2.8985 \times 10^{-3} m_\pi^2. \quad (33)$$

where $T_s \approx 150 \text{ MeV}$ is the temperature of the emitting source, $\Delta \mathcal{P}_H = \mathcal{P}_\Lambda - \mathcal{P}_{\bar{\Lambda}}$ is the difference in global polarizations of Λ and $\bar{\Lambda}$ hyperons, and $\mu_\Lambda = -\mu_{\bar{\Lambda}} = -0.613\mu_N$. In the three standard deviations (3σ) limit, the magnetic field strength is estimated as $e|B| < 1.8021 \times 10^{-2} m_\pi^2$ [94]. Here we choose m_π as the mass of π^0 meson rather than that of π^\pm , which is consistent with the pion mass that we use throughout this paper. Therefore, one can immediately use these possible constraints to compare with the magnetic field strength estimated from the extended KMW model and that from the original KMW model both in the vacuum in Fig. 2 and in the conducting medium in Fig. 3, which may enable us to make some estimations of the possible lifetime t_B of the generated magnetic field in Au+Au collisions at $\sqrt{s} = 200 \text{ GeV}$.

By comparing with the possible constraints shown by two dashed horizontal lines at 1σ and 3σ limits in Fig. 2 and Fig. 3, we notice that the magnetic field strength in the pure vacuum in Fig. 2 at a possible lifetime $t_s \simeq 5 \text{ fm}/c$ of the QGP in Au+Au collisions at $\sqrt{s} = 200 \text{ GeV}$ from hydrodynamic simulations [114] is extremely smaller than the 1σ bound of the possible constraint from the polarization data. This means that although we have improved the estimation of time evolution of the magnetic field strength by using the extended KMW model in the vacuum, which can prolong the lifetime of magnetic field to some extent, the resulting strength of the magnetic field at thermal freeze-out time $t = t_s$ still appears quite inadequate (about two orders of magnitude smaller) for explaining the observed difference between global polarizations of Λ and $\bar{\Lambda}$ hyperons. Hence, this indicates that the generated QGP in heavy-ion collisions need to maintain the magnetic field stronger for a longer lifetime than that in the vacuum, which further requires that the generated QGP is more likely a conducting medium.

In Fig. 3, as we expected above, we surprisingly notice that the magnetic field strength in the pure conducting medium with a constant electric conductivity $\sigma_0 = 5.8 \text{ MeV}$ at $3 < t < 5 \text{ fm}/c$ almost lies between the 1σ and 3σ bounds. At thermal freeze-out time $t = t_s \simeq 5 \text{ fm}/c$, we find that the magnetic field strength at impact parameter $b = 4 - 12 \text{ fm}$ lie between $eB \simeq (2.7094 - 7.8672) \times 10^{-3} m_\pi^2$, which roughly matches the required strength of magnetic field for the explanation of observed difference between global polarizations of Λ and $\bar{\Lambda}$ hyperons. Our results may support that the generated pure QGP is more likely a conducting medium, such that adequate field strength of magnetic field can be maintained until the thermal freeze-out time t_s .

In Fig. 4, we show the time evolution of the total magnetic field strength during the QGP evolution with a step-function-like electric conductivity $\tilde{\sigma} = \sigma_0 \cdot \theta(t_{\text{ret}} - t_\sigma)$ (denoted as “Mixed”) from the extended KMW model in Eqs. (27-31), which has contributions coming from both the charged sources in the vacuum and those in the pure medium. To make a better comparison, we also show the corresponding results in the pure vacuum in Fig. 2 (denoted as “Pure Vac.”) and those in the pure conducting medium in Fig. 3 (denoted as “Pure Med.”). We notice that at early-time stages the magnetic field strength during the QGP evolution are mostly contributed by charged sources in the pure vacuum ($\tilde{\sigma} = 0$), compared with which the medium effects are negligible, thus the differences between the solid lines (Mixed) and the corresponding dashed lines (Pure Vac.) are almost indistinguishable. At later-time stages, however, the medium feedback effects start to work, the resulting magnetic field strength receives growing larger contributions from the charged sources in the conducting QGP medium, which can be clearly reflected in the differences between the pure vacuum results and the mixed results. More specifically at later-time stages like $3.0 < t < 5.0 \text{ fm}/c$, we indeed check that for smaller impact parameter b it is mainly the contributions of participants in the conducting

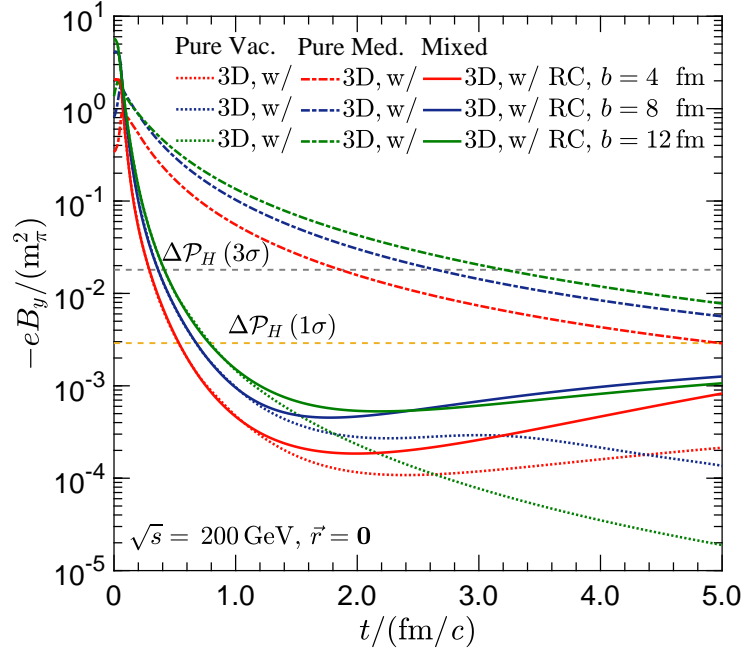


FIG. 4: (Color online) Comparison of the time evolution of the total magnetic field strength during the QGP evolution with a step-function-like electric conductivity $\tilde{\sigma} = \sigma_0 \theta(t_{\text{ret}} - t_\sigma)$ (denoted as “Mixed”) from the extended KMW model with that in the pure vacuum in Fig. 2 (denoted as “Pure Vac.”) and that in the pure conducting medium in Fig. 3 (denoted as “Pure Med.”) at different impact parameters $b = 4, 8, 12$ fm for the center point $\mathbf{r} = \mathbf{0}$ in Au+Au collisions at $\sqrt{s} = 200$ GeV. The two dashed horizontal lines indicate the later-time constraints of the magnetic field strength estimated in [94] from the difference between global polarizations of Λ and $\bar{\Lambda}$ hyperons in Au+Au collisions at $\sqrt{s} = 200$ GeV in [112] at one standard deviation (1σ) and three standard deviations (3σ), respectively.

medium that help to enhance the magnetic field strength; for larger impact parameter b , however, we find it is mainly the contributions of spectators in the conducting medium that help to enhance the magnetic field strength. Also, we notice that the contributions of spectators in the conducting medium start to appear earlier for large impact parameter b , for which the starting time can roughly be estimated as $t \simeq R_A - b/2$.

Some of these features of magnetic field strength in Fig. 4 are similar to the results in Ref. [14, 18, 20]. For $0.1 < t < 1.2$ fm/c, the mixed results are always much smaller than the pure medium results. For even later stages, e.g. $1.2 < t < 5.0$ fm/c, one can notice that the mixed results are asymptotically growing to the results in the pure medium. The behaviors of pure vacuum results at later-time stages are quite different from the mixed results especially for large impact parameter b , since the pure vacuum results are mainly due to the baryon-stopping effect while the mixed results are mainly due to the medium feedback effects.

Therefore at thermal freeze-out time t_s , the field strength of magnetic field for an relatively realistic QGP evolution from Eqs. (27-31) in the extended KMW model can well satisfy and roughly approach the 1σ constraint for the explanation of experimentally observed difference between global polarizations of Λ and $\bar{\Lambda}$ hyperons at $\sqrt{s} = 200$ GeV. Hence, our formulation of extended KMW model seems experimentally sound and reasonable, supporting that the generated QGP is most likely a conducting medium.

One thing we have neglected is that the conductivity σ in lattice QCD results should have a medium temperature T dependence, which has been parameterized and explored in Ref. [19]. Since it is known that the temperature of QGP is decreasing as the QGP fireball is expanding, the electric conductivity σ should decrease with time during the realistic QGP evolution. For such a more complicated case, we postpone it to our future study.

B. Impact Parameter Dependence of the Magnetic Field Strength

Let us now compare the impact parameter b dependence of magnetic field strength in the pure vacuum and in the pure conducting QGP medium. In Fig. 5, we show the impact parameter b dependence of the estimated magnetic field strength in the vacuum from the extended KMW model and that from the original KMW model with and without retardation correction at the center point $\mathbf{r} = \mathbf{0}$ of the overlapping region in Au+Au collisions at $\sqrt{s} = 200$ GeV at

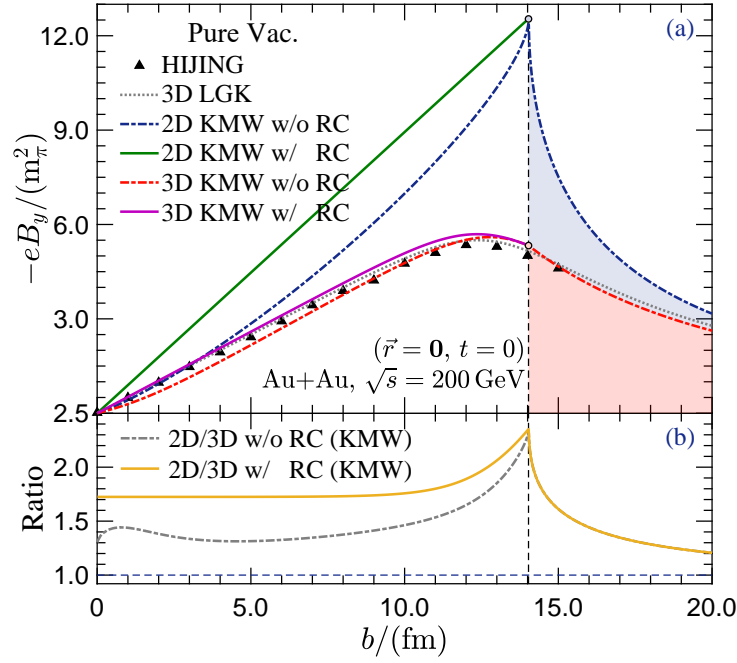


FIG. 5: (Color online) (a) Comparison of impact parameter b dependence of the estimated total magnetic field strength in the vacuum at the center point $\mathbf{r} = \mathbf{0}$ of the overlapping region in Au+Au collisions at $\sqrt{s} = 200$ GeV at $t = 0$ fm/c from six different approaches. (b) The corresponding ratio (2D/3D) of the total magnetic field strength from 2D and 3D KMW models with (w/) and without (w/o) retardation correction (RC). The dashed vertical line indicates the boundary at $b = 2R_A$, above which the two colliding nuclei will miss each other and there is no contribution from participants, as indicated by the colored bands. The corresponding “kinks” are also marked by the points along the dashed vertical line.

$t = 0$. Meanwhile, we also show the results from numerical simulations with HIJING model in [10, 51] and that from a sample analytical approach (denote as LGK model) initially proposed in [16], both of which have been used for the comparison of impact parameter dependence of magnetic field in Ref. [51].

At first glance, one may notice that the magnetic field strength in the vacuum at smaller impact parameter b from the 3D KMW model seems to deviate a lot from the results obtained with HIJING model in [10]. Meanwhile, the LGK model seems to work well and be consistent with the HIJING results. Here we should point out however that when using the HIJING model in [10] to calculate the generated magnetic field strength at $t = 0$ when the two colliding nuclei are completely overlapping with each other, all nucleons inside the two colliding nuclei are assigned with the same beam velocity $v_z^2 = 1 - (2m_N/\sqrt{s})^2$, and a similar treatment has also been employed in the LGK model [51] that all moving charges inside the two colliding nuclei are regarded as spectators. Both two methods neglect the baryon-junction stopping effect during the overlapping process. Unlike these two approaches, we have included the baryon-junction stopping effect through the experimentally supported $f_{\pm}(Y)$ in Eq. (12) in the extended KMW model, along with the generalized charge distribution. Therefore, it is not surprising that the simulation with HIJING model and the LGK model in [51] can roughly yield very similar results, and both two approaches yield slightly larger magnetic field strength especially at smaller impact parameter b due to larger charged bulk matter of participants affected by $f_{\pm}(Y)$, compared with that from the extended KMW model without retardation correction. When the retardation correction is included, however, the extended KMW model with retardation correction give a slightly larger magnetic field strength at larger impact parameter b than that from the HIJING and LGK approaches, which may be mainly attributed to the generalized charge distribution for the incorporation of Lorentz contraction effect on the geometries of the two colliding nuclei used in the extended KMW model.

In Fig. 5, one may notice the “kinks” at the boundary $b = 2R_A$ from both original and extended KMW models. That is because the two colliding nuclei begins to miss each other and there is no contribution from participants (which will be demonstrated in the following Fig. 6), compared with the other two models that seem to smoothly across the boundary. The “kinks” are due to the fact that the charge number densities in both 2D and 3D KMW models are accompanied with the step functions Θ_{\pm} so as to constrain that the charges are limited within the two colliding nuclei (with radius R_A before the Lorentz contraction), i.e. Eq. (1). Here we note that the HIJING model uses an relatively (too) large upper limit of the nucleus radius for the corresponding sampled protons inside, which actually largely exceeds the generally supposed nucleus charge radius R_c estimated from the nucleus root mean square

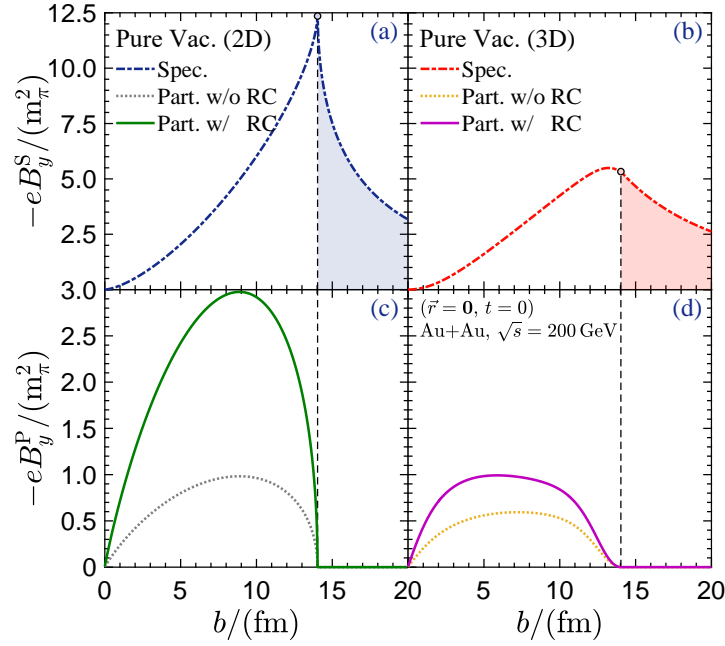


FIG. 6: (Color online) Comparison of impact parameter b dependence of the magnetic field strength in the pure vacuum contributed by spectators (S) in the upper panels (a) and (b), and that by participants (P) in the lower panels (c) and (d) at the center point $\mathbf{r} = \mathbf{0}$ of the overlapping region in Au+Au collisions at $\sqrt{s} = 200$ GeV at $t = 0$ fm/c from original (2D) KMW model (left panels) with that from extended (3D) KMW model (right panels). The dashed vertical lines indicate the boundary at $b = 2R_A$, above which the two colliding nuclei will miss each other and there is no contribution from participants, as indicated by the colored bands. The corresponding “kinks” are also marked by the points along the dashed vertical lines.

(RMS) charge radius R_{rms} measured in experiments [115], i.e. $R_A \simeq R_c = \sqrt{5/3}R_{\text{rms}}$. Similarly, the LGK model used in [51] also employs an relatively (too) large nuclear charge radius R_c in the treatment of effective charge Z_{eff} .

Besides, one can clearly notice that, compared with other three 3D models used in Fig. 5, the original KMW model indeed largely overestimates the magnetic field strength at $t = 0$, which corresponds to the too sharp cusp of magnetic field strength around $t \sim 0$ especially at large impact parameter b in Fig. 2. This can be roughly attributed to the more localized and central elevated 2D surface charge number density and no longitudinal position dependence of the EM fields in the original KMW model. Moreover, we show the ratios (2D/3D) of the total estimated magnetic field strength from the original KMW model to that from the extended KMW model with and without retardation correction in the lower panel of Fig. 5. One can clearly see that the original KMW overestimates the magnetic field strength roughly by a factor of ~ 1.7 (1.5) at relatively smaller impact parameter b with (without) retardation correction, and by a factor of ~ 2.4 (2.4) at the boundary $b = 2R_A$ in particular.

In Fig. 6, we make a detailed comparison of the impact parameter b dependence of the estimated magnetic field strength in the pure vacuum contributed by spectators and participants from the original KMW model with that from the extended KMW model with and without retardation correction. From the upper panels of Fig. 6, one can clearly see that it is mainly the contributions of spectators in the original KMW model that cause the too shape peak of the estimated magnetic field strength, compared with that result from the extended KMW model, which is also consistent with observed too shape cusp during the time evolution in Fig. 5 around $t \sim 0$.

In the lower panels of Fig. 6, we also notice that the magnetic field strength contributed by participants with retardation correction systematically shows strong enhancements relative to that without retardation correction for both 2D and 3D KMW models. This is mainly due to the fact that the baryon-junction stopping effect represented by $f_{\pm}(Y)$ in Eq. (14) is basically ruled out by the $\theta(t_{\text{ret}} - t_c)$ function during the comparison between retardation time t_{ret} and collision time t_c . The contributions of charged participants actually are all calculated with beam rapidity $\pm Y_0$ instead of the normalized rapidity distribution $f_{\pm}(Y)$. Hence this kind of enhancement is quite significant at $t = 0$, especially for the 2D KMW model due to the more localized 2D surface charge number density. It is quite noticeable that the magnetic field strength contributed by participants in the 3D KMW model for a middle impact parameter b , e.g., $b = 8$ fm, is almost one third of that in the 2D KMW model for the case with retardation correction.

Different from the situation in the pure vacuum in Fig. 5, the centrality dependence of the generated magnetic field strength in the conducting medium should be realistically evaluated at some time after the collision, since the formation of equilibrated pure QGP medium certainly needs some time after the collision time t_c . At present, it is still not very

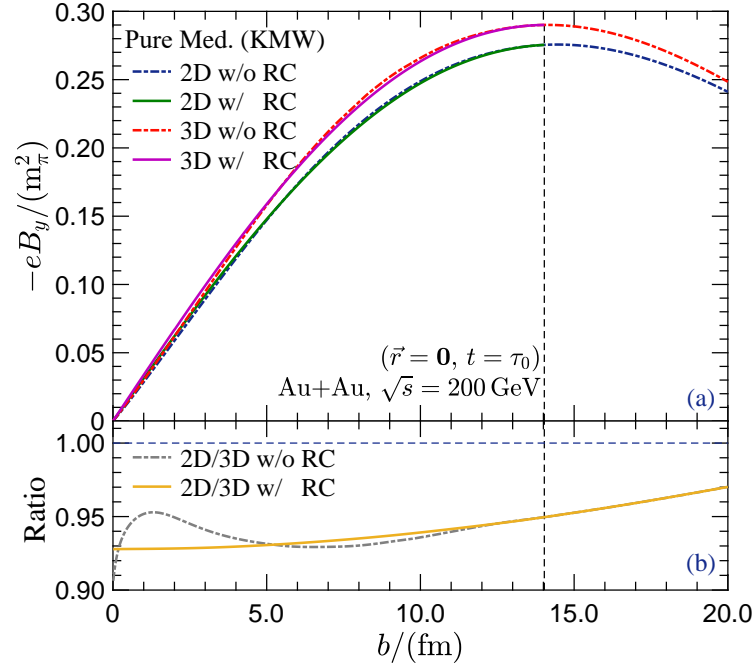


FIG. 7: (Color online) (a) Comparison of impact parameter b dependence of the total magnetic field strength in the pure conducting QGP medium at hydrodynamical (pre-) equilibration time $t = \tau_0 = 0.6 \text{ fm}/c$ [114, 116] with a constant Ohm electric conductivity $\sigma_0 = 5.8 \text{ MeV}$ from extended (3D) KMW model and that from original (2D) KMW model at the center point $\mathbf{r} = \mathbf{0}$ of the overlapping region in Au+Au collisions at $\sqrt{s} = 200 \text{ GeV}$. (b) The corresponding ratio (2D/3D) of the total magnetic field strength from 2D and 3D KMW models with (w/) and without (w/o) retardation correction (RC). The dashed vertical line indicates the boundary at $b = 2R_A$ in Fig. 5, compared to which there is no “kink” at all since the two colliding nuclei have already missed each other before $t = \tau_0$ and the corresponding shaded color bands are also not shown.

clear how long it takes for the formation of equilibrated pure QGP medium in heavy-ion collisions, so we estimate it from the widely used (pre-) equilibration time in hydrodynamical simulations, namely $t = \tau_0 = 0.6 \text{ fm}/c$ [114, 116].

In Fig. 7, we show the impact parameter b dependence of the estimated total magnetic field strength in the pure conducting QGP medium at $t = \tau_0 = 0.6 \text{ fm}/c$ [114, 116] with a constant electric conductivity $\sigma_0 = 5.8 \text{ MeV}$ from the extended KMW model and that from the original KMW model at the center point $\mathbf{r} = \mathbf{0}$ of the overlapping region in Au+Au collisions at $\sqrt{s} = 200 \text{ GeV}$. One can see that the difference between the original KMW model and the extended KMW model at $t = \tau_0$ in the pure conducting medium is not as significant as that case at $t = 0$ in the vacuum in Fig. 5. From the lower panel of Fig. 7, we can also see that the extended KMW model systematically yields a relatively stronger total magnetic field strength than the original KMW model for the conducting medium at $t = \tau_0$, which is distinctly different from the situation in the vacuum case at $t = 0$ in Fig. 5. This is resulted from the delay of the generated magnetic field in the conducting medium according to the Faraday’s induction law since a constant Ohm electric conductivity σ_0 has been explicitly embedded into the Maxwell’s equations in Eq. (15). Moreover, there is no longer any “kink” at $t = \tau_0$ in Fig. 7, since the two colliding nuclei have already departed from each other at the estimated t_d in Eq. (32).

Likewise, we show in Fig. 8 a detailed comparison of the impact parameter b dependence of the estimated magnetic field strength in the pure conducting QGP medium contributed by spectators and participants at $t = \tau_0 = 0.6 \text{ fm}/c$ [114, 116] with a constant electric conductivity $\sigma_0 = 5.8 \text{ MeV}$ from the original KMW model with that from the extended KMW model with and without retardation correction. In the upper panels of Fig. 8, one can clearly see that the original KMW model and the extended KMW model can give almost the same impact parameter b dependent magnetic field strength contributed by spectators, although the result in the extended KMW model is slightly stronger. In the lower panels of Fig. 8, we find that the retardation correction can only mildly modulate the impact parameter b dependent magnetic field strength contributed by participants in the conducting medium, which is more noticeably stronger in the extended KMW model than that in the original KMW model, similar to the situation of spectators in the upper panels of Fig. 8. These behaviors in the conducting medium, however, are distinctly different from those in the vacuum at $t = 0 \text{ fm}/c$ in Fig. 6 where the original KMW model will systematically yield a stronger magnetic field strength than the extended KMW model.

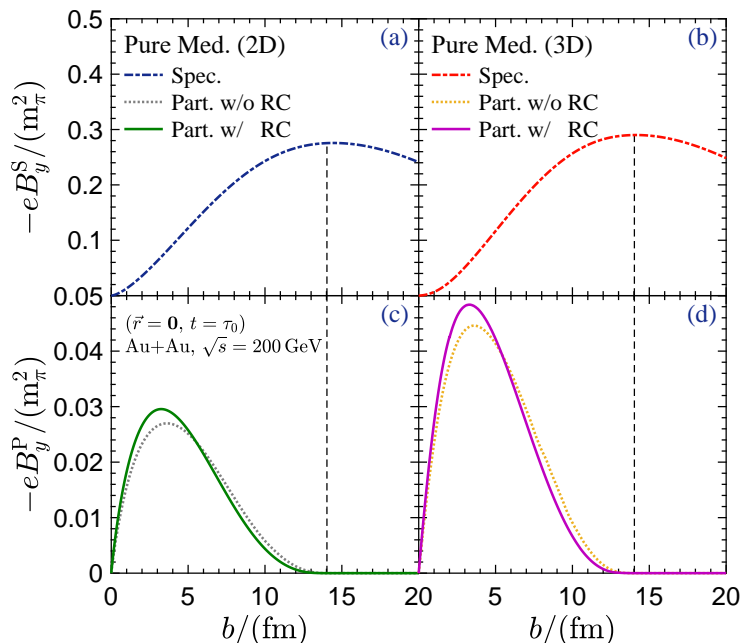


FIG. 8: (Color online) Comparison of impact parameter b dependence of the magnetic field strength in the pure conducting QGP medium contributed by spectators (S) in the upper panels (a) and (b), and that by participants (P) in the lower panels (c) and (d) at hydrodynamical (pre-) equilibration time $t = \tau_0 = 0.6 \text{ fm}/c$ [114, 116] with a constant Ohm electric conductivity $\sigma_0 = 5.8 \text{ MeV}$ at the center point $\mathbf{r} = \mathbf{0}$ fm of the overlapping region in Au+Au collisions at $\sqrt{s} = 200 \text{ GeV}$ from original (2D) KMW model (left panels) with that from extended (3D) KMW model (right panels). The dashed vertical lines indicate the boundary at $b = 2R_A$ in Fig. 5, compared to which there is no “kink” at all since the two colliding nuclei have already missed each other before $t = \tau_0$ and the corresponding shaded color bands are also not shown.

IV. SUMMARY

In summary, based on the Kharzeev-McLerran-Warringa (KMW) model [2] for the estimation of strong EM fields generated in relativistic heavy-ion collisions, we make an attempt to generalize the formulas of estimated EM fields in the original KMW model, which eventually turns out to be above formulations in the extended KMW model.

We first start from generalizing the widely used charge distribution (or charge number density) models by incorporating the Lorentz contraction effect for the ellipsoidal geometry of each colliding nucleus due to relativistic motion, e.g., the three-parameter Fermi (3pF) model, for both spherically symmetric colliding nuclei as well as axially deformed colliding nuclei used in heavy-ion collisions. We then combine the widely used L-W equations of EM fields with the generalized three-dimensional (3D) charge number densities. By employing the decomposition method for the contributions of spectators and participants as that in the original KMW model [2], we then naturally generalize the formulas of EM fields in the vacuum by incorporating the longitudinal position dependence and retardation correction (RC) for heavy-ion collisions.

Since the medium feedback effects in the conducting QGP medium may substantially modify the time evolution of the generated EM fields according to the Faraday’s induction law, we then explicitly and analytically embed a constant Ohm electric conductivity σ_0 into the Maxwell’s equations for the incorporation of medium effects, and eventually formulate the estimation of generated EM fields with medium effects in the extended KMW model for a pure conducting medium and for a realistic QGP medium. For simplicity, we also propose one possible kind of simplification of the formulas of EM fields in the realistic QGP medium in APPENDIX A, which can serve as an alternative solution to doing Monte-Carlo simulations of generated EM fields from widely used L-W equations for heavy-ion collisions.

Our formulations of the estimated EM fields in the extended KMW model can result in a slower time evolution (or longer lifetime $t_B \sim 5 \text{ fm}/c$) and a more reasonable impact parameter b dependence of the magnetic field strength in the vacuum. The inclusion of medium feedback effects through a constant electric conductivity $\sigma_0 = 5.8 \text{ MeV}$ from lattice QCD results in the pure medium and a time-dependent conductivity in the realistic QGP medium further helps to prolong the time evolution of the magnetic field. We surprisingly find the magnetic field strength at thermal freeze-out time well satisfy the required field strength and roughly approach the 1σ limit for the explanation of the

observed difference in global polarizations of Λ and $\bar{\Lambda}$ hyperons in Au+Au collisions at $\sqrt{s} = 200$ GeV. This feature may to some extent indicate that the generated QGP is more likely a conducting medium, such that stronger field strength of magnetic field can be maintained until the thermal freeze-out time t_s .

It should be emphasized that our generalization of charge distributions with the three-parameter Fermi model (3pF) that we present in this paper is actually a sample example, many other charge distribution models that are listed in [96] or somewhere else for various colliding nuclei can be similarly generalized in the same way as we present here.

Last but not least, the extended KMW model can be potentially applied to various colliding energies, especially for the lower energy regions like the ongoing STAR-BES program and the under planning FAIR, NICA and J-PARC programs. Hopefully, these generalized formulations in the extended KMW model can be employed for many EM fields relevant studies, such as the CME related charge asymmetry correlators or fluctuations in the experimental searching, the in-medium particle's mass as well as QCD phase diagram under strong magnetic field, and so on.

Acknowledgments

The authors would like to gratefully thank Yu-Gang Ma, Jin-Hui Chen, Song Zhang and Qi-Ye Shou for their stimulating and helpful discussions and comments, and Chen Zhong for maintaining high-quality performance of computational facilities. Y. C. thankfully acknowledges the helpful and fruitful discussions with Wei-Tian Deng, Huan-Xiong Yang, Heng-Tong Ding, Xu-Guang Huang, and Qun Wang, as well as the timely discussions and helps from Xin-Li Zhao, Xin Ai, Bang-Xiang Chen, Yu Guo, Xiao-Liang Xia, Hui Li and Xian-Gai Deng. Y. C. and G.-L. M. are supported by National Natural Science Foundation of China (NSFC) under Grants Nos. No. 11890710, 11890714, 11835002, and 11961131011, the Strategic Priority Research Program of Chinese Academy of Sciences under Grant No. XDB34030000, and the Guangdong Major Project of Basic and Applied Basic Research under Grant No. 2020B0301030008. X.-L. S. is supported by National Natural Science Foundation of China (NSFC) under Grant Nos. 11890714 and 12047528.

APPENDIX A. ALTERNATIVE SOLUTION TO THE ESTIMATED EM FIELDS IN SIMULATIONS

Due to the ellipsoidal-type geometry and also peculiar charge domains occupied by spectators and participants, the numerical integrations of charge distributions for the estimated EM fields from Eqs. (10-14) in the pure vacuum, Eqs. (22-26) in the pure medium and Eqs. (27-31) during the QGP evolution are actually not very easily and quickly performed. Meanwhile, we notice that the L-W equations of EM fields in the vacuum, i.e. Eq. (8), are widely accepted and used. We therefore propose one possible simplification of the formulas of EM fields during the QGP evolution from Eqs. (27-31) by replacing the continuous integrations of charge distributions with the discrete summation for all point-like charges, which turns out to be an alternative solution to doing Monte-Carlo numerical simulations of generated EM fields from L-W equations [3, 5, 8–11, 15, 21–23, 29–34] as follows

$$\begin{aligned} e\mathbf{B}_S^\pm(t, \mathbf{r}) &= \lim_{Y \rightarrow \pm Y_0} \alpha_{\text{EM}} \sum_{N_S} Z_n \frac{\sinh(Y) \cdot \mathbf{e}_z \times \mathbf{R}_\pm}{\Delta^{3/2}} \left[1 + \frac{\tilde{\sigma} \sinh|Y|}{2} \sqrt{\Delta} \right] e^{\tilde{A}}, \\ e\mathbf{B}_P^\pm(t, \mathbf{r}) &= \alpha_{\text{EM}} \sum_{N_P} Z_n \int_{-Y_0}^{Y_0} dY \frac{\Psi_\pm(Y) \sinh Y \cdot \mathbf{e}_z \times \mathbf{R}_\pm}{\Delta^{3/2}} \left[1 + \frac{\tilde{\sigma} \sinh|Y|}{2} \sqrt{\Delta} \right] e^{\tilde{A}}, \end{aligned} \quad (\text{A.1})$$

for the decomposed magnetic field \mathbf{B} contributed by spectators and participants. For that of the electric field \mathbf{E} , we obtain the following expressions for x and y components of the electric field E_x and E_y ,

$$\begin{aligned} \begin{pmatrix} eE_{x,S}^\pm \\ eE_{y,S}^\pm \end{pmatrix} (t, \mathbf{r}) &= \lim_{Y \rightarrow \pm Y_0} \alpha_{\text{EM}} \sum_{N_S} Z_n \left\{ \frac{R_\perp \cosh Y}{\Delta^{3/2}} \left(1 + \frac{\tilde{\sigma} \sinh |Y|}{2} \sqrt{\Delta} \right) \right. \\ &\quad \left. - \frac{\tilde{\sigma}}{R_\perp \tanh |Y|} \left[1 + \frac{\sinh |Y|}{\sqrt{\Delta}} \left(t - \frac{z - z'}{\tanh Y} \right) \right] \exp \left(-\tilde{\sigma} \left[t - \frac{z - z'}{\tanh Y} \right] \right) \right\} \frac{e^{\tilde{A}}}{R_\perp} \begin{pmatrix} x - x' \\ y - y' \end{pmatrix}, \\ \begin{pmatrix} eE_{x,P}^\pm \\ eE_{y,P}^\pm \end{pmatrix} (t, \mathbf{r}) &= \alpha_{\text{EM}} \sum_{N_P} Z_n \int_{-Y_0}^{Y_0} dY \Psi_\pm(Y) \left\{ \frac{R_\perp \cosh Y}{\Delta^{3/2}} \left(1 + \frac{\tilde{\sigma} \sinh |Y|}{2} \sqrt{\Delta} \right) \right. \\ &\quad \left. - \frac{\tilde{\sigma}}{R_\perp \tanh |Y|} \left[1 + \frac{\sinh |Y|}{\sqrt{\Delta}} \left(t - \frac{z - z'}{\tanh Y} \right) \right] \exp \left(-\tilde{\sigma} \left[t - \frac{z - z'}{\tanh Y} \right] \right) \right\} \frac{e^{\tilde{A}}}{R_\perp} \begin{pmatrix} x - x' \\ y - y' \end{pmatrix}, \end{aligned} \quad (\text{A.2})$$

and also that for the z component of the electric field E_z ,

$$\begin{aligned} eE_{z,S}^\pm(t, \mathbf{r}) &= \lim_{Y \rightarrow \pm Y_0} \alpha_{\text{EM}} \sum_{N_S} Z_n \left\{ \frac{\text{sgn}(Y) \tilde{\sigma}^2}{\tanh^2 Y} \exp \left(-\tilde{\sigma} \left[t - \frac{z - z'}{\tanh Y} \right] \right) \Gamma(0, -\tilde{A}) \right. \\ &\quad \left. + \frac{e^{\tilde{A}}}{\Delta^{3/2}} \left[(z - z') \cosh Y - t \sinh Y - \text{sgn}(Y) \tilde{A} \sqrt{\Delta} - \frac{\tilde{\sigma} \sinh Y}{\tanh^2 Y} \Delta \right] \right\}, \\ eE_{z,P}^\pm(t, \mathbf{r}) &= \alpha_{\text{EM}} \sum_{N_P} Z_n \int_{-Y_0}^{Y_0} dY \Psi_\pm(Y) \left\{ \frac{\text{sgn}(Y) \tilde{\sigma}^2}{\tanh^2 Y} \exp \left(-\tilde{\sigma} \left[t - \frac{z - z'}{\tanh Y} \right] \right) \Gamma(0, -\tilde{A}) \right. \\ &\quad \left. + \frac{e^{\tilde{A}}}{\Delta^{3/2}} \left[(z - z') \cosh Y - t \sinh Y - \text{sgn}(Y) \tilde{A} \sqrt{\Delta} - \frac{\tilde{\sigma} \sinh Y}{\tanh^2 Y} \Delta \right] \right\}. \end{aligned} \quad (\text{A.3})$$

Here the expressions for R_\perp , Δ and \tilde{A} are the same as the definitions in Eq. (29), and $\Psi_\pm(Y)$ in Eq. (14). N_S and N_P denote the total numbers of spectators and participants of point-like charges, respectively. Also, we note that a similar Monte-Carlo simulation using above formulas of EM fields for point-like charges in Eqs. (A.1-A.3) has firstly been performed in [24], since such an alternative formulation could have been more directly obtained from the EM fields of point-like charge in [24] when further embedded with the refined baryon-junction stopping effect with retardation correction as in Eq. (14) and step-function-like conductivity $\tilde{\sigma} = \sigma_0 \cdot \theta(t_{\text{ret}} - t_\sigma)$.

If one assumes that each proton can be treated as point-like charge, as has been extensively assumed in literatures [3, 5, 8–11, 15, 21, 23, 29–34], then above generalization of EM fields in Eqs. (A.1-A.3) for Monte-Carlo simulations in heavy-ion collisions can have at least two merits: one is that the EM fields from Eqs. (A.1-A.3) are analytically embedded with a step-function-like electric conductivity $\tilde{\sigma}$ for the incorporation of medium effects during the QGP evolution rather than the original L-W equations in the vacuum; the other is that the EM fields in Eqs. (A.1-A.3) are also implanted with the refined baryon-junction stopping effect with retardation correction as in Eq. (14).

-
- [1] J. Rafelski and B. Muller, Phys. Rev. Lett. **36**, 517 (1976), <https://doi.org/10.1103/PhysRevLett.36.517>.
 - [2] D. E. Kharzeev, L. D. McLerran, and H. J. Warringa, Nucl. Phys. A **803**, 227 (2008), <https://doi.org/10.1016/j.nuclphysa.2008.02.298>, arXiv:0711.0950[hep-ph].
 - [3] V. Skokov, A. Y. Illarionov, and V. Toneev, Int. J. Mod. Phys. A **24**, 5925 (2009), <https://doi.org/10.1142/S0217751X09047570>, arXiv:0907.1396[nucl-th].
 - [4] Kirill Tuchin, Phys. Rev. C **82**, 034904 (2010); Phys. Rev. C **83**, 039903 (2011), <https://doi.org/10.1103/PhysRevC.83.039903>, <https://doi.org/10.1103/PhysRevC.82.034904>, arXiv:1006.3051[nucl-th].
 - [5] Sergei A. Voloshin, Phys. Rev. Lett. **105**, 172301 (2010), <http://dx.doi.org/10.1103/PhysRevLett.105.172301>, arXiv:1006.1020[nucl-th].
 - [6] M. Asakawa, A. Majumder, and B. Müller, Phys. Rev. C **81**, 064912 (2010), <http://dx.doi.org/10.1103/PhysRevC.81.064912>, arXiv:1003.2436[hep-ph].
 - [7] V. Voronyuk, V. D. Toneev, W. Cassing, E. L. Bratkovskaya, V. P. Konchakovski, and S. A. Voloshin, Phys. Rev. C **83**, 054911 (2011), <http://dx.doi.org/10.1103/PhysRevC.83.054911>, arXiv:1103.4239[nucl-th].
 - [8] L. Ou and B. A. Li, Phys. Rev. C **84**, 064605 (2011), <http://dx.doi.org/10.1103/PhysRevC.84.064605>, arXiv:1107.3192[nucl-th].
 - [9] A. Bzdak and V. Skokov, Phys. Lett. B **710**, 171 (2012), <https://doi.org/10.1016/j.physletb.2012.02.065>, arXiv:1111.1949[hep-ph].

- [10] Wei-Tian Deng and Xu-Guang Huang, Phys. Rev. C **85**, 044907 (2012), <http://dx.doi.org/10.1103/PhysRevC.85.044907>, arXiv:1201.5108[nucl-th].
- [11] V. D. Toneev, V. P. Konchakovski, V. Voronyuk, E. L. Bratkovskaya, and W. Cassing, Phys. Rev. C **86**, 064907 (2012), <http://dx.doi.org/10.1103/PhysRevC.86.064907>, arXiv:1208.2519[nucl-th].
- [12] V. D. Toneev, V. Voronyuk, E. L. Bratkovskaya, W. Cassing, V. P. Konchakovski, and S. A. Voloshin, Phys. Rev. C **85**, 034910 (2012), <https://doi.org/10.1103/PhysRevC.85.034910>, arXiv:1112.2595[hep-ph].
- [13] Kirill Tuchin, Phys. Rev. C **88**, 024911 (2013), <https://doi.org/10.1103/PhysRevC.88.024911>, arXiv:1305.5806[hep-ph].
- [14] Kirill Tuchin, Adv. High Energy Phys. **2013**, 490495 (2013), <http://dx.doi.org/10.1155/2013/490495>, arXiv:1301.0099[hep-ph].
- [15] John Błoczynski, Xu-Guang Huang, Xilin Zhang, and Jinfeng Liao, Phys. Lett. B **718**, 1529 (2013), <http://dx.doi.org/10.1016/j.physletb.2012.12.030>, arXiv:1209.6594[nucl-th].
- [16] Yunpeng Liu, Carsten Greiner, and Che Ming Ko, arXiv:1403.4317[nucl-th].
- [17] Umut Gursoy, Dmitri Kharzeev, and Krishna Rajagopal, Phys. Rev. C **89**, 054905 (2014), <http://dx.doi.org/10.1103/PhysRevC.89.054905>, arXiv:1401.3805[hep-ph].
- [18] L. McLerran and V. Skokov, Nucl. Phys. A **929**, 184 (2014), <http://dx.doi.org/10.1016/j.nuclphysa.2014.05.008>, arXiv:1305.0774[hep-ph].
- [19] B. G. Zakharov, Phys. Lett. B **737**, 266 (2014), <http://dx.doi.org/10.1016/j.physletb.2014.08.068>, arXiv:1404.5047[hep-ph].
- [20] Kirill Tuchin, Phys. Rev. C **93**, 014905 (2015), <https://doi.org/10.1103/PhysRevC.93.014905>, arXiv:1508.06925[hep-ph].
- [21] Wei-Tian Deng and Xu-Guang Huang, Phys. Lett. B **742**, 296 (2014), <http://dx.doi.org/10.1016/j.physletb.2015.01.050>, arXiv:1411.2733[nucl-th].
- [22] John Błoczynski, Xu-Guang Huang, Xilin Zhang, and Jinfeng Liao, Nucl. Phys. A **939**, 85 (2015), <http://dx.doi.org/10.1016/j.nuclphysa.2015.03.012>, arXiv:1311.5451[nucl-th].
- [23] V. Roy and S. Pu, Phys. Rev. C **92**, 064902 (2015), <http://dx.doi.org/10.1103/PhysRevC.92.064902>, arXiv:1508.03761[nucl-th].
- [24] Hui Li, Xin-li Sheng, and Qun Wang, Phys. Rev. C **94**, 044903 (2016), <http://dx.doi.org/10.1103/PhysRevC.94.044903>, arXiv:1602.02223[nucl-th].
- [25] Robert Holliday, Ryan McCarty, Balthazar Peroutka, and Kirill Tuchin, Nucl. Phys. A **957**, 406 (2017), <http://dx.doi.org/10.1016/j.nuclphysa.2016.10.003>, arXiv:1604.04572[hep-ph].
- [26] Balthazar Peroutka and Kirill Tuchin, Nucl. Phys. A **966**, 64 (2017), <http://dx.doi.org/10.1016/j.nuclphysa.2017.05.104>, arXiv:1704.04485[nucl-th].
- [27] Duan She, Sheng-Qin Feng, Yang Zhong, and Zhong-Bao Yin, Eur. Phys. J. A **54**, 48 (2018), <https://doi.org/10.1140/epja/i2018-12481-x>, arXiv:1709.04662[hep-ph].
- [28] Umut Gursoy, Dmitri Kharzeev, Eric Marcus, Krishna Rajagopal, and Chun Shen, Phys. Rev. C **98**, 055201 (2018), <https://doi.org/10.1103/PhysRevC.98.055201>, arXiv:1806.05288[hep-ph].
- [29] Xin-Li Zhao, Yu-Gang Ma, and Guo-Liang Ma, Phys. Rev. C **97**, 024910 (2018), <https://doi.org/10.1103/PhysRevC.97.024910>, arXiv:1709.05962[hep-ph].
- [30] Xin-Li Zhao, Guo-Liang Ma, and Yu-Gang Ma, Phys. Lett. B **792**, 413 (2019), <https://doi.org/10.1016/j.physletb.2019.04.002>, arXiv:1901.04156[hep-ph].
- [31] Xin-Li Zhao, Guo-Liang Ma, and Yu-Gang Ma, Phys. Rev. C **99**, 034903 (2019), <https://doi.org/10.1103/PhysRevC.99.034903>, arXiv:1901.04151[hep-ph].
- [32] Yi-Lin Cheng, Song Zhang, Yu-Gang Ma, Jin-Hui Chen, and Chen Zhong, Phys. Rev. C **99**, 054906 (2019), <https://doi.org/10.1103/PhysRevC.99.054906>, arXiv:1909.03160[nucl-th].
- [33] Jan Hammelmann, Alba Soto-Ontoso, Massimiliano Alvioli, Hannah Elfner, and Mark Strikman, Phys. Rev. C **101**, 061901(R) (2020), <https://doi.org/10.1103/PhysRevC.101.061901>, arXiv:1908.10231[nucl-th].
- [34] X. G. Deng and Y. G. Ma, Phys. Rev. C **101**, 054610 (2020), <https://doi.org/10.1103/PhysRevC.101.054610>, arXiv:2006.00718[nucl-th].
- [35] Bang-Xiang Chen, and Sheng-Qin Feng, Chin. Phys. C **42**, 024104 (2020), <https://doi.org/10.1088/1674-1137/44/2/024104>, arXiv:1909.10836[hep-ph].
- [36] E. V. Shuryak, Phys. Rept. **61**, 71 (1980), [https://doi.org/10.1016/0370-1573\(80\)90105-2](https://doi.org/10.1016/0370-1573(80)90105-2).
- [37] P. Braun-Munzinger, K. Redlich, J. Stachel, in *Quark Gluon Plasma 3*, ed. by R. C. Hwa, X.-N. Wang, World Scientific, Singapore (2004), <https://doi.org/10.1142/5029>.
- [38] J. Adams *et al.* (STAR Collaboration), Nucl. Phys. A **757**, 102 (2005), <https://doi.org/10.1016/j.nuclphysa.2005.03.085>, arXiv:nucl-ex/0501009.
- [39] Adam Bzdak, Shin'ichi Esumi, Volker Koch, Jin-feng Liao, Mikhail Stephanov, and Nu Xu, Phys. Rept. **853**, 1 (2020), <https://doi.org/10.1016/j.physrep.2020.01.005>, arXiv:1906.00936[nucl-th].
- [40] A. A. Belavin, A. M. Polyakov, A. S. Shvarts and Yu. S. Tyupkin, Phys. Lett. B **59**, 85 (1975), [https://doi.org/10.1016/0370-2693\(75\)90163-X](https://doi.org/10.1016/0370-2693(75)90163-X).
- [41] G. 't Hooft, Phys. Rev. Lett. **37**, 8 (1976); Phys. Rev. D **14**, 3432 (1976); Phys. Rev. D **18**, 2199 (1978), <https://doi.org/10.1103/PhysRevLett.37.8>, <https://doi.org/10.1103/PhysRevD.14.3432>, <https://doi.org/10.1103/PhysRevD.18.2199.3>.
- [42] R. Jackiw and C. Rebbi, Phys. Rev. Lett. **37**, 172 (1976), <https://doi.org/10.1103/PhysRevLett.37.172>.

- [43] Kenji Fukushima, Dmitri E. Kharzeev, and Harmen J. Warringa, Phys. Rev. D **78**, 074033 (2008), <http://dx.doi.org/10.1103/PhysRevD.78.074033>, arXiv:0808.3382[hep-ph].
- [44] Harmen J. Warringa, J. Phys. G: Nucl. Part. Phys. **35** (2008) 104012, <http://dx.doi.org/10.1088/0954-3899/35/10/104012>, arXiv:0805.1384[hep-ph].
- [45] Dmitri E. Kharzeev and Harmen J. Warringa, Phys. Rev. D **80**, 034028 (2009), <http://dx.doi.org/10.1103/PhysRevD.80.034028>, arXiv:0907.5007[hep-ph].
- [46] Kenji Fukushima, Dmitri E. Kharzeev, and Harmen J. Warringa, Nucl. Phys. A **836**, 311 (2010), <https://doi.org/10.1016/j.nuclphysa.2010.02.003>, arXiv:0912.2961[hep-ph].
- [47] Kenji Fukushima, Dmitri E. Kharzeev, and Harmen J. Warringa, Phys. Rev. Lett. **104**, 212001 (2010), <http://dx.doi.org/10.1103/PhysRevLett.104.212001>, arXiv:1002.2495[hep-ph].
- [48] Dmitri E. Kharzeev, Ann. Phys. **353**, 205 (2010), <https://doi.org/10.1016/j.aop.2009.11.002>, arXiv:0911.3715[hep-ph].
- [49] Dmitri Kharzeev, Karl Landstriner, Andreas Schmitt, and Ho-Ung Yee (ed.), *Lect. Notes Phys.*, **871**, 1-624 (2013), <https://doi.org/10.1007/978-3-642-37305-3>.
- [50] Dmitri E. Kharzeev, Prog. Part. Nucl. Phys. **75**, 133 (2014), <https://doi.org/10.1016/j.ppnp.2014.01.002>, arXiv:1312.3348[hep-ph].
- [51] Koichi Hattori and Xu-Guang Huang, Nucl. Sci. Tech. **28**, 26 (2017), <https://doi.org/10.1007/s41365-016-0178-3>, arXiv:1609.00747[nucl-th].
- [52] V. P. Gusynin, V. A. Miransky and I. A. Shovkovy, Phys. Rev. Lett. **73**, 3499 (1994); Phys. Rev. Lett. **76**, 1005 (1996), <https://doi.org/10.1103/PhysRevLett.73.3499>, <https://doi.org/10.1103/PhysRevLett.76.1005>, arXiv:hep-ph/9405262.
- [53] A. J. Mizher, M. N. Chernodub, and E. S. Fraga, Phys. Rev. D **82**, 105016 (2010), <https://doi.org/10.1103/PhysRevD.82.105016>, arXiv:1004.2712[hep-ph].
- [54] Hao-Lei Chen, Kenji Fukushima, Xu-Guang Huang, and Kazuya Mameda, Phys. Rev. D **93**, 104052 (2016), <https://doi.org/10.1103/PhysRevD.93.104052>, arXiv:1512.08974[hep-ph].
- [55] Claudio Bonati, Massimo D'Elia, Marco Mariti, Michele Mesiti, Francesco Negro, Andrea Rucci, and Francesco Sanfilippo, Phys. Rev. D **95**, 074515 (2017), <https://doi.org/10.1103/PhysRevD.95.074515>, arXiv:1703.00842[hep-lat].
- [56] G. S. Bali, B. B. Brandt, G. Endrodi, and B. Glässle, Phys. Rev. D **97**, 034505 (2018), <https://doi.org/10.1103/PhysRevD.97.034505>, arXiv:1707.05600[hep-lat].
- [57] M. Coppola, D. Gomez Dumm, and N. N. Scoccola, Phys. Lett. B **782**, 155 (2018), <https://doi.org/10.1016/j.physletb.2018.04.043>, arXiv:1802.08041[hep-ph].
- [58] Shijun Mao, Phys. Rev. D **99**, 056005 (2019), <https://doi.org/10.1103/PhysRevD.99.056005>, arXiv:1808.10242[nucl-th].
- [59] E. J. Ferrer and A. Sanchez, Phys. Rev. D **100**, 096006 (2019), <https://doi.org/10.1103/PhysRevD.100.096006>, arXiv:1910.11245[hep-ph].
- [60] H.-T. Ding, S.-T. Li, A. Tomiya, X.-D. Wang, and Y. Zhang, arXiv:2008.00493[hep-lat].
- [61] J. O. Andersen, W. R. Naylor and A. Tranberg, Phys. Rev. Lett. **100**, 032007 (2008), <https://doi.org/10.1103/RevModPhys.88.025001>, arXiv:1411.7176[hep-ph].
- [62] Stefan Rechenberger, Phys. Rev. D **95**, 054013 (2017), <https://doi.org/10.1103/PhysRevD.95.054013>, arXiv:1612.07541[hep-ph].
- [63] Massimo D'Elia, Floriano Manigrasso, Francesco Negro, and Francesco Sanfilippo, Phys. Rev. D **98**, 054509 (2018), <https://doi.org/10.1103/PhysRevD.98.054509>, arXiv:1808.07008[hep-lat].
- [64] Guo-yun Shao, Wei-bo He, and Xue-yan Gao, Phys. Rev. D **100**, 014020 (2019), <https://doi.org/10.1103/PhysRevD.100.014020>, arXiv:1907.02201[hep-ph].
- [65] Shile Chen, Jiaxing Zhao, and Pengfei Zhuang, arXiv:2005.08473[nucl-th].
- [66] D. T. Son and M. A. Stephanov, Phys. Rev. D **77**, 014021 (2008), <https://doi.org/10.1103/PhysRevD.77.014021>, arXiv:0710.1084[hep-ph].
- [67] S. A. Voloshin, Phys. Rev. C **70**, 057901 (2004), <https://doi.org/10.1103/PhysRevC.70.057901>, arXiv:hep-ph/0406311.
- [68] I. V. Selyuzhenkov, (STAR Collaboration), Rom. Rep. Phys. **58**, 049 (2006), <http://rrp.infm.ro/>, arXiv:nucl-ex/0510069.
- [69] B. I. Abelev *et al.* (STAR Collaboration), Phys. Rev. Lett. **103**, 251601 (2009), <https://doi.org/10.1103/PhysRevLett.103.251601>, arXiv:0909.1739[nucl-ex].
- [70] B. I. Abelev *et al.* (STAR Collaboration), Phys. Rev. C **81**, 054908 (2010), <https://doi.org/10.1103/PhysRevC.81.054908>, arXiv:0909.1717[nucl-ex].
- [71] S. A. Voloshin, (STAR Collaboration), Indian J. Phys. **85**, 1103 (2011), <https://doi.org/10.1007/s12648-011-0137-0>, arXiv:0806.0029[nucl-ex].
- [72] G. Wang, (STAR Collaboration), Nucl. Phys. A **248**, 904 (2013), <http://dx.doi.org/10.1016/j.nuclphysa.2013.01.069>, arXiv:1210.5498[nucl-ex].
- [73] L. Adamczyk *et al.* (STAR Collaboration), Phys. Rev. Lett. **113**, 052302 (2014), <https://doi.org/10.1103/PhysRevLett.113.052302>, arXiv:1404.1433[nucl-ex].
- [74] B. I. Abelev *et al.* (ALICE Collaboration), Phys. Rev. Lett. **110**, 012301 (2013), <https://doi.org/10.1103/PhysRevLett.110.012301>, arXiv:1207.0900[nucl-ex].
- [75] F. Wang, Phys. Rev. C **81**, 064902 (2010), <https://doi.org/10.1103/PhysRevC.81.064902>, arXiv:0911.

- 1482[nucl-ex].
- [76] A. Bzdak, V. Koch, and J. Liao, Phys. Rev. C **81**, 031901 (2010), <https://doi.org/10.1103/PhysRevC.81.031901>, arXiv:0912.5050[nucl-th].
 - [77] J. Liao, V. Koch, and A. Bzdak, Phys. Rev. C **82**, 054902 (2010), <https://doi.org/10.1103/PhysRevC.82.054902>, arXiv:1005.5380[nucl-th].
 - [78] A. Bzdak, V. Koch, and J. Liao, Phys. Rev. C **83**, 014905 (2011), <https://doi.org/10.1103/PhysRevC.83.014905>, arXiv:1008.4919[nucl-th].
 - [79] S. Pratt, arXiv:1002.1758[nucl-th].
 - [80] S. Schlichting and S. Pratt, arXiv:1005.5341[nucl-th].
 - [81] S. Schlichting, S. Pratt, Phys. Rev. C **83**, 014913 (2011), <https://doi.org/10.1103/PhysRevC.83.014913>, arXiv:1009.4283[nucl-th].
 - [82] S. Pratt, S. Schlichting, and S. Gavin, Phys. Rev. C **84**, 024909 (2011), <https://doi.org/10.1103/PhysRevC.84.024909>, arXiv:1011.6053[nucl-th].
 - [83] A. Bzdak, V. Koch, and J. Liao, Lect. Notes Phys. **871**, 503 (2013), <https://doi.org/10.1007/978-3-642-37305-3>, arXiv:1207.7327[nucl-th].
 - [84] Wei-Tian Deng, Xu-Guang Huang, Guo-Liang Ma, and Gang Wang, Phys. Rev. C **94**, 041901 (2016), <https://doi.org/10.1103/PhysRevC.94.041901>, arXiv:1607.04697[nucl-th].
 - [85] V. Koch, S. Schlichting, V. Skokov, P. Sorensen, J. Thomas, S. Voloshin, G. Wang, and H.-U. Yee, Chin. Phys. C **41**, 072001 (2017), <https://doi.org/10.1088/1674-1137/41/7/072001>, arXiv:1608.00982[nucl-th].
 - [86] Xu-Guang Huang, Wei-Tian Deng, Guo-Liang Ma, and Gang Wang, Nucl. Phys. A **967**, 736 (2017), <https://doi.org/10.1016/j.nuclphysa.2017.05.071>, arXiv:1704.04382[nucl-th].
 - [87] Shuzhe Shi, Yin Jiang, Elias Lilleskov, and Jinfeng Liao, Ann. Phys. **394**, 50 (2018), <https://doi.org/10.1016/j.aop.2018.04.026>, arXiv:1711.02496[nucl-th].
 - [88] Hao-jie Xu, Xiaobao Wang, Hanlin Li, Jie Zhao, Zi-Wei Lin, Caiwan Shen, and Fuqiang Wang, Phys. Rev. Lett. **121**, 022301 (2018), <https://doi.org/10.1103/PhysRevLett.121.022301>, arXiv:1710.03086[nucl-th].
 - [89] Shu-zhe Shi, Hui Zhang, De-fu Hou, and Jin-feng Liao, Phys. Rev. Lett. **125**, 242301 (2020), <https://doi.org/10.1103/PhysRevLett.125.242301>, arXiv:1910.14010[nucl-th].
 - [90] Dmitri Kharzeev, Phys. Lett. B **633**, 260 (2006), <https://doi.org/10.1016/j.physletb.2005.11.075>, arXiv:hep-ph/0406125.
 - [91] Dmitri Kharzeev and Ariel Zhitnitsky, Nucl. Phys. A **797**, 67 (2007), <https://doi.org/10.1016/j.nuclphysa.2007.10.001>, arXiv:0706.1026[hep-ph].
 - [92] C. G. Callan, R. F. Dashen, D. J. Gross, Phys. Lett. B **63**, 334 (1976), [https://doi.org/10.1016/0370-2693\(76\)90277-X](https://doi.org/10.1016/0370-2693(76)90277-X).
 - [93] Evan Stewart and Kirill Tuchin, Phys. Rev. C **97**, 044906 (2018), <https://doi.org/10.1103/PhysRevC.97.044906>, arXiv:1710.08793[nucl-th].
 - [94] Berndt Müller and Andreas Schäfer, Phys. Rev. D **98**, 071902 (2018), <https://doi.org/10.1103/PhysRevD.98.071902>, arXiv:1806.10907[hep-ph].
 - [95] Q. Y. Shou, Y. G. Ma, P. Sorensen, A. H. Tang, F. Videbæk, and H. Wang, Phys. Lett. B **749**, 215 (2015), <http://dx.doi.org/10.1016/j.physletb.2015.07.078>, arXiv:1409.8375[nucl-th].
 - [96] H. De Vries, C. W. De Jager, and C. De Vries, Atom. Data Nucl. Data Tabl. **36**, 495 (1987), [https://doi.org/10.1016/0092-640X\(87\)90013-1](https://doi.org/10.1016/0092-640X(87)90013-1).
 - [97] F. J. Ernst, R. G. Sachs and K. C. Wali, Phys. Rev. **119**, 1105 (1960), <https://doi.org/10.1103/PhysRev.119.1105>.
 - [98] M. L. Miller, K. Reygers, S. J. Sanders, and P. Steinberg, Annu. Rev. Nucl. Part. Sci. **57**, 205 (2007), <https://doi.org/10.1146/annurev.nucl.57.090506.123020>, arXiv:nucl-ex/0701025.
 - [99] D. Kharzeev, Phys. Lett. B **378**, 238 (1996), [https://doi.org/10.1016/0370-2693\(96\)00435-2](https://doi.org/10.1016/0370-2693(96)00435-2), arXiv:nucl-th/9602027.
 - [100] G. C. Rossi and G. Veneziano, Nucl. Phys. B **123**, 507 (1977), [https://doi.org/10.1016/0550-3213\(77\)90178-X](https://doi.org/10.1016/0550-3213(77)90178-X).
 - [101] L. Montanet, G. C. Rossi and G. Veneziano, Phys. Rep. **63**, 149 (1980), [https://doi.org/10.1016/0370-1573\(80\)90161-1](https://doi.org/10.1016/0370-1573(80)90161-1).
 - [102] E. Abbas *et al.* (ALICE Collaboration), Eur. Phys. J. C **73**, 2496 (2013), <https://doi.org/10.1140/epjc/s10052-013-2496-5>, arXiv:1305.1562[nucl-ex].
 - [103] P. B. Arnold, G. D. Moore, and L. G. Yaffe, J. High Energy Phys. **05** (2003) 051, <https://doi.org/10.1088/1126-6708/2003/05/051>, arXiv:hep-ph/0302165.
 - [104] S. Gupta, Phys. Lett. B **597**, 57 (2004), <https://doi.org/10.1016/j.physletb.2004.05.079>, arXiv:hep-lat/0301006.
 - [105] G. Aarts, C. Allton, J. Foley, S. Hands, and S. Kim, Phys. Rev. Lett. **99**, 022002 (2007), <https://doi.org/10.1103/PhysRevLett.99.022002>, arXiv:hep-lat/0703008.
 - [106] H. T. Ding, A. Francis, O. Kaczmarek, F. Karsch, E. Laermann, and W. Soeldner, Phys. Rev. D **83**, 034504 (2011), <https://doi.org/10.1103/PhysRevD.83.034504>, arXiv:1012.4963[hep-lat].
 - [107] A. Francis and O. Kaczmarek, Prog. Part. Nucl. Phys. **67**, 212 (2012), <https://doi.org/10.1016/j.ppnp.2011.12.020>, arXiv:1112.4802[hep-lat].
 - [108] Alessandro Amato, Gert Aarts, Chris Allton, Pietro Giudice, Simon Hands, and Jon-Ivar Skullerud, Phys. Rev. Lett. **111**, 172001 (2013), <https://doi.org/10.1103/PhysRevLett.111.172001>, arXiv:1307.6763[hep-lat].
 - [109] B. B. Brandt, A. Francis, H. B. Meyer, and H. Wittig, J. High Energy Phys. **03** (2013) 100, [https://doi.org/10.1007/JHEP03\(2013\)100](https://doi.org/10.1007/JHEP03(2013)100), arXiv:1212.4200[hep-lat].

- [110] Yin Jiang, Shuzhe Shi, Yi Yin, and Jinfeng Liao, Chin. Phys. C **42**, 011001 (2018), <https://doi.org/10.1088/1674-1137/42/1/011001>, [arXiv:1611.04586\[nucl-th\]](#).
- [111] L. Adamczyk *et al.* (STAR Collaboration), Nature (London) **548**, 62 (2017), <https://doi.org/10.1038/nature23004>, [arXiv:1701.06657\[nucl-ex\]](#).
- [112] J. Adam *et al.* (STAR Collaboration), Phys. Rev. C **98**, 014910 (2018), <https://doi.org/10.1103/PhysRevC.98.014910>, [arXiv:1805.04400\[nucl-ex\]](#).
- [113] Yu Guo, Shu-Zhe Shi, Sheng-Qin Feng, and Jin-Feng Liao, Phys. Lett. B **798**, 134929 (2019), <https://doi.org/10.1016/j.physletb.2019.134929>, [arXiv:1905.12613\[nucl-th\]](#).
- [114] Hui-Chao Song and Ulrich Heinz, Phys. Rev. C **77**, 064901 (2008), <https://doi.org/10.1103/PhysRevC.77.064901>, [arXiv:0712.3715\[nucl-th\]](#).
- [115] I. Angeli and K. P. Marinova, Atom. Data Nucl. Data Tabl. **99**, 69 (2013), <https://doi.org/10.1016/j.adt.2011.12.006>.
- [116] Peter F. Kolb and Ralf Rapp, Phys. Rev. C **67**, 044903 (2003), <https://doi.org/10.1103/PhysRevC.67.044903>, [arXiv:hep-ph/0210222](#).